REVIEW

Check for updates

Dissolution of pozzolanic materials: a critical review

Mohammadreza Izadifar, [ID] *[a] Reza Khorshidi,[b] Neven Ukrainczyk, [ID] [a] Reyhaneh Alborz [ID] [c] and Eduardus Koenders [ID] [a]

The construction industry is a major source of carbon emissions, driven largely by the production of conventional Portland cement. Reducing this footprint calls for replacing energy- and emission-intensive clinker with supplementary cementitious materials. Pozzolanic sources such as metakaolin (MK), ground granulated blast furnace slag (GGBFS), and fly ash (FA) offer a viable pathway to low-carbon binders when their activation mechanisms are fully optimized. This review synthesizes and integrates recent advances in the activation and valorization of these materials into sustainable aluminosilicate binders. It examines how precursor structure, calcination parameters, activator chemistry, and curing conditions govern dissolution kinetics, gel formation, and resulting microstructure. Experimental findings are complemented by multi-scale computational approaches, density functional theory (DFT), molecular dynamics (MD), and coarse-grained Monte Carlo (CGMC) simulations, providing atomic- to meso-scale insight into reaction pathways and long-term structural evolution. Key results showed that calcination near 700 °C produces highly reactive metakaolin enriched in five-fold coordinated aluminum, NaOH delivers the highest dissolution rates, and sodium silicate fosters denser gel networks, while GGBFS reactivity benefits from Ca- and Mg-driven calcium–silicate–hydrates (C–S–H) formation. Increased structural disorder lowers dissolution energy barriers, enhancing activation efficiency. The integrated experimental–computational framework enables predictive optimization of precursor processing and activator selection, accelerating the development of durable, low-carbon binders from industrial byproducts and supporting the transition toward greener construction materials.

1. Introduction

Global warming and environmental constraints within the construction industry have intensified the search for low-carbon alternative binders[1–5] calcined clays[6,7] which often contain substantial amounts of metakaolin (MK, AS_2), along with byproducts of slag (GGBFS, S) and fly ash (FA, F), are increasingly utilized as supplementary cementitious materials (SCMs)[8–10] to partially replace cement clinker in mortars, concrete, and also used in geopolymer concrete.[11–20] These substitutions contribute to a reduction in overall cement production, thereby lowering carbon dioxide emissions.[21–26] The production of these aluminosilicates requires only moderate energy input, making them ideal for green concrete applications. Therefore, evaluating pozzolanic reactions is crucial to

determining the extent to which cement can be substituted with SCMs[11,23,27–32]

It is important to clearly distinguish between pozzolanic reactions and alkali-activation (geopolymerization) processes, as these mechanisms differ fundamentally in their chemistry and reaction products. Pozzolanic reactions occur in calcium-rich environments, where aluminosilicate precursors such as MK, FA, or GGBFS react with calcium hydroxide to form calcium-bearing hydrates, primarily C–S–H and C–A–S–H. In contrast, alkali-activation involves the dissolution of aluminosilicate precursors in highly alkaline solutions (*e.g.*, NaOH, KOH, or alkali silicates), followed by polycondensation reactions that lead to the formation of alkali aluminosilicate gels such as C–(N–)A–S–H. In this review, both reaction routes are discussed where relevant, with explicit differentiation between their dissolution mechanisms, reaction pathways, and binding phases.

Pozzolanic reactivity is important as it allows materials to participate in chemical reactions that improve the overall performance and durability of construction materials. Various parameters are commonly used to assess pozzolanic reactivity, including reactive silicon dioxide (SiO_2, S) content,

[a] Institute of Construction and Building Materials, Technical University of Darmstadt, Franziska-Braun-Str. 3, 64287, Darmstadt, Germany. E-mail: izadifar@wib.tu-darmstadt.de, mr.izadifar@icloud.com

[b] Department of Materials and Earth Sciences, Technical University of Darmstadt, Otto-Berndt-Strasse 3, 64287, Darmstadt, Germany

[c] Department of Chemical and Bioengineering, Friedrich-Alexander-Universität Erlangen-Nürnberg (FAU), Germany

the consumption of calcium oxide (CaO, C) or calcium hydroxide (CH), the relative strength index, and the concentration of soluble silicon (Si) and aluminum (Al) ions in an alkaline solution.[7,33,34] Additionally, factors such as the pozzolanic to alkali ratio, curing time, curing temperature, pH, water/solid ratio, and the structure of the pozzolan structure itself are important considerations.[29,35–37]

MK, as a pozzolanic material, can react with CH generated during cement hydration. The pozzolanic activity of MK in Portland cement (PC) systems is commonly examined through the simplified MK–CH system. Previous research on the MK–CH system has identified calcium–silicate–hydrates (C–S–H)[38–44] and calcium–alumino–silicate–hydrates (C–A–S–H),[45,46] as the primary pozzolanic reaction products.[47] These reaction products are essential for binding within the cementitious matrix, thereby directly contributing to improved mechanical strength.[48–52] The reactivity of pozzolan determines both the rate and the extent of C–S–H formation. Since C–S–H is the primary binding phase in concrete, higher pozzolan reactivity results in a denser and stronger matrix by filling micropores and decreasing overall porosity, thereby enhancing both the compressive strength and durability of the material.[6,8,53–55] Factors, such as curing time, temperature, alkali concentration, and pH significantly influence both the reactivity and the mechanical properties of cementitious materials.

Curing temperature is crucial in the concrete setting, particularly in accelerating pozzolanic reactions. At ambient temperatures, these reactions proceed slowly, but initial curing at elevated temperatures can significantly enhance the reaction rates, especially when the system's chemical composition is optimized.[56,57] Brooks reported[58] that increasing the temperature from 6 to 80 °C, shortened the setting time by a factor of six due to the accelerated pozzolanic reactivity in FA. Additionally, curing temperatures in the range of 30 to 90 °C have also been shown to improve concrete's compressive strength.[59] Palomo et al.[60] observed that curing FA at 85 °C for 5 hours resulted in a mechanical strength of 60 MPa. They emphasized that the temperature is particularly crucial during the first 2 to 5 hours of the curing process. Kirschner et al.[61] demonstrated that ambient temperature curing was impractical for MK in geopolymerization due to delayed setting; however, curing at 75 °C for 4 hours allowed a significant portion of the geopolymerization process to complete. Thus, curing at elevated temperatures, especially within the 30 to 90 °C range, is highly effective and plays a crucial role in enhancing geopolymerization.[29]

Extended curing time enhances the polymerization process, leading in higher compressive strength. However, strength gains beyond 48 hours of curing are minimal.[59,60,62] Conversely, curing at elevated temperatures for prolonged periods reduces compressive strength, as extended heat exposure disrupts the granular structure of the geopolymer matrix. This disruption leads to dehydration and excessive shrinkage due to gel contraction, preventing the transformation into a more stable semi-crystalline form.[56,63]

In terms of alkaline concentration and pH, aluminosilicate solubility rises with increasing hydroxide ion concentration,

and higher alkalinity levels typically lead to greater compressive strength.[56,64] Wang et al.[65] observed that high sodium hydroxide (NaOH, NH) addition to cement klin dust (CKD)-FA binders accelerates the chemical dissolution process, while inhibiting the formation of ettringite (Aft, $C_6As_3H_{32}$), and CH during binder hydration as confirmed by X-ray diffraction (XRD) measurements. However, addition of OH^- concentration can reduce overall strength of the system.[60] They further reported that adding 5% NaOH boosts early-age binder strength (under 7 days), but this binder strength declines at later ages due to excessive NaOH, which leads to undesirable morphologies and non-uniform hydration products within the pastes. The setting time of cement decreases as the pH of the activating solution increases. At higher pH levels, the mixture forms a more fluid gel composition with reduced viscosity and improved workability.[66] Elevated pH favors the formation of smaller chain oligomers and monomeric silicates $(SiO_4)^{4-}$, which react more readily with soluble Al.[66,67] Conversely, at lower pH, the geopolymeric mix is more viscous, behaving similarly to a paste from cement mixing. This results in a reduced concentration of reactive monomers, leading to a thicker, less fluid mixture.[66]

The term "geopolymer", coined by Davidovits in 1978,[68] denotes materials formed by combining aluminosilicate powder with a precursor solution of potassium silicate (KS, K–S) or sodium silicate (NS, N–S).[69,70]

The geopolymerization reaction can be divided into three stages: (I) dissolution: raw materials are dissolved in an alkaline solution, releasing $(SiO_4)^{4-}$ and aluminate $Al(OH)_4^-$ reactive species. (II) Transportation and Orientation: The dissolved monomers are transported and oriented to form polymeric Si–O–Si (–Al)–O linkages through the sharing of oxygen atoms. (III) Polycondensation: This stage involves the polycondensation process, where these linkages build a reticular crosslinking structure, resulting in the formation of the geopolymer.[70–72]

Any pozzolanic compound or source of SiO_2 and Al_2O_3 that readily dissolves in an alkaline solution can serve as a source of geopolymer precursor species, making it suitable for geopolymerization.[73,74]

Si-rich materials, such as FA and rice husk ash (RHA, R), along with calcium-rich materials like GGBFS and Al-rich materials such as thermally-activated kaolin and bentonite clays, are essential to the geopolymerization process.[70,75,76] Additionally, other materials, such as ordinary PC and kiln dust, can be used as reactive fillers or setting additives, which contribute to the development of favorable mechanical properties.[77] Table 1 shows the chemical compositions of a number of pozzolans.[78]

The alkali component used as an activator in geopolymerization typically consists of compounds derived from elements in group 1 of the periodic table. As a result, materials produced through this process are commonly referred to as alkali-activated aluminosilicate binders or alkali-activated cementitious materials.[11,79,80] Strong alkalis are essential for activation of the S and Al in pozzolanic materials and setting additives, facilitating the partial or complete transformation of the glassy

Table 1 Chemical compositions of various pozzolans.[78] Reproduced with permission from Elsevier Science & Technology Journals © 2001 (permission conveyed through Copyright Clearance Center, Inc.)[78]

Pozzolan	Mass percentage							
	SiO_2	Al_2O_3	Fe_2O_3	CaO	MgO	$Na_2O + K_2O$	SO_3	LOI
PC	21.0	4.63	2.26	65.6	1.18	0.94	—	0.99
GGBFS	34.0	16.0	0.32	36.92	8.83	0.87	2.67	0.0
FA	49.1	26.4	9.3	1.4	1.4	5.0	0.8	4.9
SF	92.0	0.7	1.2	0.2	0.2	2.0	—	3.0
MK	52.1	41.0	4.32	0.07	0.19	0.89	—	0.6
Ground clay brick	54.83	19.05	6.0	9.39	1.77	3.65	2.9	1.48

structure into a highly compacted composite. Common activators used for this purpose include NaOH, sodium sulfate (Na_2SO_4, NS), NS, sodium carbonate (Na_2CO_3, NC), potassium carbonate (K_2CO_3, KC), potassium hydroxide (KOH, KH), and potassium sulfate (K_2SO_4, KS). The more alkalis comes into contact with the reactive solid material, the greater the release of $(SiO_4)^{4-}$ and $Al(OH)_4^-$ reactive species.[60,64,81–84] On the other hand, gel binder, produced from a mixture of pozzolanic materials used as SCMs together with cement clinker, are classified into two categories:[11]

(1) Calcium-rich binders: these are synthesized from calcium-rich materials, such as GGBFS. When activated with an alkaline solution CH, they produce C–(A–)S–H gel.

(2) Low-calcium, high-silica, and alumina binders: these binders are made from materials that are low in calcium but rich in SiO_2 and alumina (Al_2O_3, A), such as MK. When activated with an alkaline solution CH, they form C–A–S–H network, which develops high mechanical strength at early ages, especially when subjected to mild thermal curing.

Atomistic computational methods have recently emerged as a powerful tool for understanding the microstructure of cement and its relationship to reactivity.[31,85–97] Techniques such as MD,[98–107] DFT,[108–110] and CGMC[111–113] computational approaches are extensively employed in chemistry and materials science to investigate properties reaction mechanisms, mechanical properties, as well as activation and bonding energies. Computational modeling approaches like MD and DFT provide valuable insights into the chemical reaction processes underlying geopolymerization at the molecular level. Through MDs simulation, the behavior of each element involved in the reaction can be closely tracked, enabling detailed observation of each stage in the geopolymerization process.[71,90] This review focuses on the dissolution behavior and reactivity of pozzolanic materials, based on insights from both experimental studies and computational methods, including MD, DFT, and CGMC. It provides a comprehensive survey of the literatures published up to August 2025, encompassing peer-reviewed articles and review papers published in English-language journals. The scope of the review includes studies that address key mechanisms of dissolution, reaction kinetics, and microstructural changes in pozzolanic materials when exposed to alkaline environments. By synthesizing a broad range of studies, this review aims to offer a foundational reference for researchers in the field of pozzolanic material reactivity and dissolution behavior, as well as a guide for advancing computational approaches in these domains. For clarity and consistency, all component abbreviations, idealized chemical formulas, and short notation used throughout this review are

Table 2 Idealized chemical formulas and abbreviations of components used throughout this review article

Component	Chemical formula	Short notation	Abbreviation
Kaolinite	$Al_2Si_2O_5(OH)_4$	AS_2H_4	Kln
Metakaolin	$Al_2O_3 \cdot 2SiO_2$	AS_2	MK
Slag	$(CaO)–(SiO_2)–(Al_2O_3)–(MgO)$	S	GGBFS
Fly ash	$(SiO_2)–(Al_2O_3)–(Fe_2O_3)$	F	FA
Rice husk ash	SiO_2	R	RHA
Calcium hydroxide	$Ca(OH)_2$	CH	CH
Calcium carbonate	$CaCO_3$	Cc	Cc
Sodium silicate	Na_2SiO_3	N-S	NS
Sodium hydroxide	NaOH	NH	NaOH
Potassium silicate	K_2SiO_3	K-S	KS
Potassium hydroxide	KOH	KH	KOH
Sodium sulfate	Na_2SO_4	NS	Na_2SO_4
Sodium carbonate	Na_2CO_3	NC	Na_2CO_3
Potassium carbonate	K_2CO_3	KC	K_2CO_3
Potassium sulfate	K_2SO_4	KS	K_2SO_4
Tetra-calcium aluminate hydrate	$4CaO \cdot Al_2O_3 \cdot 13H_2O$	C_4AH_{13}	CAH_{13}
Ettringite	$Ca_6Al_2(SO_4)_3(OH)_{12} \cdot 26H_2O$	$C_6As_3H_{32}$	AFt
Monosulfoaluminate	$Ca_4Al_2(SO_4)(OH)_{12} \cdot 6H_2O$	C_4AsH_{12}	Ms (AFm)
Silicon dioxide	SiO_2	S	SiO_2
Calcium oxide	CaO	C	CaO
Alumina	Al_2O_3	A	Al_2O_3
Magnesium oxide	MgO	M	MgO

Table 3 Priority research topic & key question

Topics	Key research questions to be solved
Transformation of kaolinite to MK and structural influences	How do calcination conditions, Si/Al ratio, and surface area affect MK's dissolution and reactivity in alkaline environments?
Composition, structure, and dissolution factors	How do variations in chemical composition, amorphicity, particle size, and activator type/concentration control dissolution mechanisms?
Quantum and nanoscale computational modeling of pozzolanic materials	How can atomistic simulations be refined to more accurately capture dissolution pathways and better align with experimental findings?
Cross-material analysis and optimization	What are the optimal activation conditions for MK, FA, and GGBFS, and how can standardized methodologies enable reliable cross-comparisons?

summarized in Table 2. Each abbreviation is also defined at its first occurrence in the text to ensure unambiguous interpretation. Key topics from this introduction alongside research gaps and key questions that remain to be addressed in each area are summarized in Table 3.

2. Focus and constrains

The aim of this review is to provide a state of the art on the available fundamental knowledge on dissolution and reactivity of key pozzolanic materials, namely MK, GGBFS, and FA in various alkaline activation environments. By integrating both theoretical perspectives and experimental findings, this review precisely aims to clarify the fundamental reaction mechanisms of these materials in simplified systems, with a particular focus on the effects of primary activators such as NaOH, KOH, KS, and CH. Although this study primarily focuses on the MK, GGBFS, and FA systems, it deliberately excludes the complexities of multi-binder systems (*e.g.*, blended cements), thereby facilitating a more focused analysis of each material's intrinsic reactivity.

The review is organized into four main sections. It begins by examining the transformation of kaolinite (Kln, AS_2H_4) into MK through calcination, emphasizing the critical intermediate dehydroxylated phase, which disrupts the crystalline structure and results in an amorphous form that significantly enhances reactivity. Important structural factors such as the Si/Al ratio, surface area, and calcination temperature are analyzed for their influence on MK's dissolution properties in alkaline environments. Additionally, the dissolution and reactivity of MK across various activators are explored, comparing its behavior in NaOH, KOH, KS, and CH. Although existing studies provide insights into MK dissolution within individual activators, there remains a notable gap in cross-activator comparisons under consistent conditions. Addressing this gap could provide crucial insights for optimizing MK reactivity and is essential for future research.

In the second section, the dissolution mechanisms and reactivity of two amorphous pozzolanic materials of FA and GGBFS, distinguished by varying levels of CaO, SiO_2 and Al_2O_3, are examined. The discussion begins with their structural compositions, highlighting the role of their aluminosilicate networks in influencing dissolution mechanism and reactivity. Key factors affecting the dissolution of FA and GGBFS are addressed, including particle size, chemical composition,

amorphicity, and the concentration and type of alkaline activator. Although a variety of activators (such as NaOH, NS, and NC) have been explored, there remains a need for more standardized methodologies and cross-comparisons, which could enhance understanding of reactivity differences across pozzolanic materials.

In the third section, MD and DFT computational approaches are discussed for studying the atomic structure and reactivity of MK, GGBFS, and FA. These advanced simulation techniques provide atomistic perspectives on dissolution, enabling a deeper look into reaction pathways, structural changes, and energy dynamics during activation. By investigating reaction mechanisms at the molecular level, computational studies provide valuable complementary insights that support experimental research, especially in examining crystallographic defects, coordination states, and ion interactions in pozzolanic reactions. Nonetheless, it is important to note that computational studies often face constraints in replicating the full complexity of real-world systems, such as scaling challenges and simplified model assumptions.[85,114,115]

In the final section, based on the findings from both experimental and computational studies, a comparative assessment of the dissolution and reactivity mechanisms of MK, GGBFS, and FA across various alkaline conditions is provided. This comparative analysis identifies key factors that influence dissolution and reactivity in each material, pointing out optimal conditions for activation. Furthermore, it highlights the strengths and limitations of each material across various applications, serving as a practical guide for future research aimed at optimizing pozzolanic performance in cementitious and alkali-activated systems. This comprehensive analysis bridges existing gaps in the literature and enhances understanding of the parameters that control pozzolanic reactions, thus paving the way for targeted advancements in both fundamental research and practical applications. Key topics, along with research gaps and outstanding questions in this area, are summarized in Table 3.

3. Kaolinite and metakaolin

3.1. Kaolinite and metakaolin structures

Kaolin, a raw material, contains Kln as one of its primary mineral phases. Kln is a 1 : 1 clay mineral with a structure consisting of one $(SiO_4)^{4-}$ sheet linked to one octahedral alumina (AlO_6) sheet, giving it pseudo-hexagonal symmetry; it

belongs to the triclinic crystal system with space group $P1$ and unit cell parameters of approximately $a = 5.15$ Å, $b = 8.95$ Å, $c = 7.40$ Å, $\alpha = 90°$, $\beta = 104.5°$, and $\gamma = 89.8°$.[116]

MK is synthesized by thermal activation *via* calcination of Kln, a process that involves dehydroxylation (DHX), and serves as a key source for producing SCMs and geopolymer precursors. DHX of Kln commonly occurs in the range of from 400 to 850 °C. In laboratory scale, calcination is typically conducted at approximately 700 °C.[117–120] Hanein *et al.*[121] also reported that the range of optimal industrial calcination temperature is between 700 and 850 °C.

During calcination, three main processes occur:

(1) Dehydration: at around 300 °C, molecular water is lost.[121]

(2) Dehydroxylation: this process begins at 350 °C and is completed by 700 °C, resulting in the removal of hydroxyl groups (OH⁻) and partially disordered structure.[6,117,121]

(3) Recrystallization: occurring above 800 °C, this process reduces the reactivity of MK with the loss of structural disorder.[6,117]

Among the stages of calcination, the dehydroxylation stage is particularly significant, as it can greatly influence the dissolution and reactivity of MK.

During dehydroxylation, the crystalline structure of MK is disrupted, giving rise to an amorphous structure[6,117,122] that significantly enhances the material's reactivity.[114,122,123] DHX of the octahedral sheet during calcination enhances surface reactivity, leading to better activation. However, excessive heating can result in particle agglomeration and the formation of non-reactive high-temperature phases, reducing their reactivity.[9,114] The temperature at which DHX occurs is influenced by three major factors: the heating conditions,[124–126] the morphology and particle size of the Kln,[120] and the stacking order of its structural layers.[21,114,120]

Studies have demonstrated that MK exhibits a variety of neighboring arrangements with Al in all three coordination states (IV, V, and VI).[76,114,127] In Kln, Al is primarily octahedrally coordinated (Al^{VI}), whereas in fully dehydroxylated MK, Al transitions predominantly to tetrahedral coordination (Al^{IV}). This occurs through interactions with two Si and two Al atoms *via* bridging oxygen. In partially dehydroxylated clay, Al is primarily five-coordinated (Al^{V}), reaching the maximum Al activity.[122,128] Fernandez *et al.*[6] highlighted that the arrangement of nearest neighbors in the MK structure is critical for its dissolution and reactivity. They proposed that modifying the short-range order of Si in MK could reduce crystallinity. This can be achieved through partial calcination at temperatures between 600 °C and 800 °C, which increases the presence of 5-fold coordinatioin Al (Al^{V}), a more reactive form than the 4-fold coordination Al (Al^{IV}) produced during complete dihydroxylation.[114,122]

Izadifar *et al.*[114] conducted an in-depth study of the structure of Kln during dehydroxylation process through comprehensive experimental and quantum-atomistic DFT computational approach. An initial periodic $1 \times 1 \times 3$ ideal and B-vacant ordered Kln supercell (Fig. 1A) was simulated, extending unit cell in z direction 3 times. Disordered Kln (Fig. 2A) was simulated by $b/3$ translation of B-vacant layers. They reported that the crystal structure and chemical bonding within each layer remain identical. Conversely, it has been demonstrated that the length of hydrogen bonds between the layers differs. This difference in hydrogen bond length is attributed to the different configurations of the layers in these minerals. Fig. 1 and 2 illustrate Kln, partially dehydroxylated Kln, MK, and scanning electron microscopics (SEMs) images of Kln and MK in ordered and disordered configurations, respectively. Fig. 3A and B illustrate the transformation of Kln into MK, where the thermodynamically stable $Al_{12}Si_{12}O_{39}(OH)_6$ phase is formed in the third stage of DHX before transforming into MK at higher temperatures. Similarly, Fig. 4A and B show the transformation of disordered Kln into metadiskaolinite, characterized by the
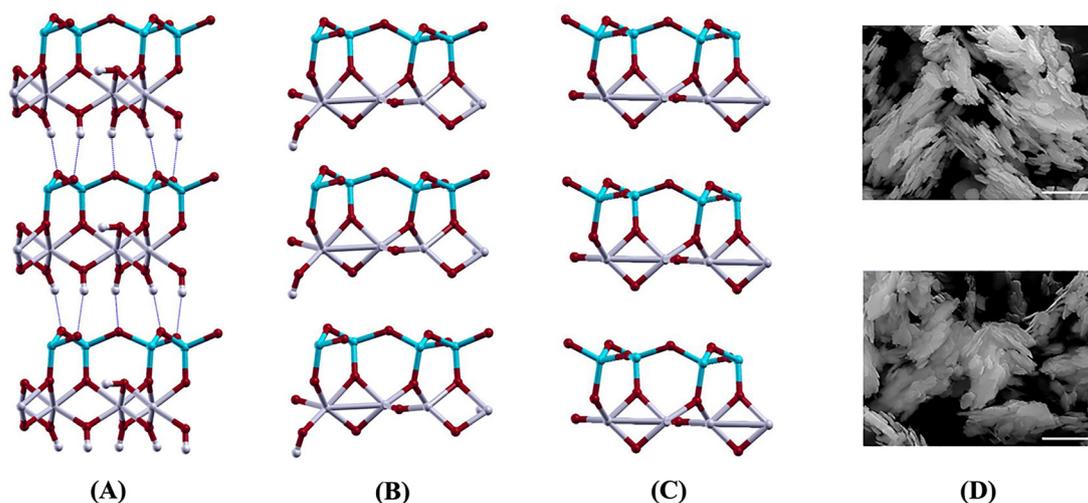

Fig. 1 (A) Kln ($Al_{12}Si_{12}O_{30}(OH)_{24}$), (B) partially dehydroxylated Kln ($Al_{12}Si_{12}O_{39}(OH)_6$), (C) MK ($Al_{12}Si_{12}O_{42}$), and (D) SEM images of ordered Kln KBEI_M2 (upper), and MK KBEI_M2 700 C (lower);[114] reproduced from Izadifar *et al.*, 2020,[114] licensed under CC BY 4.0.
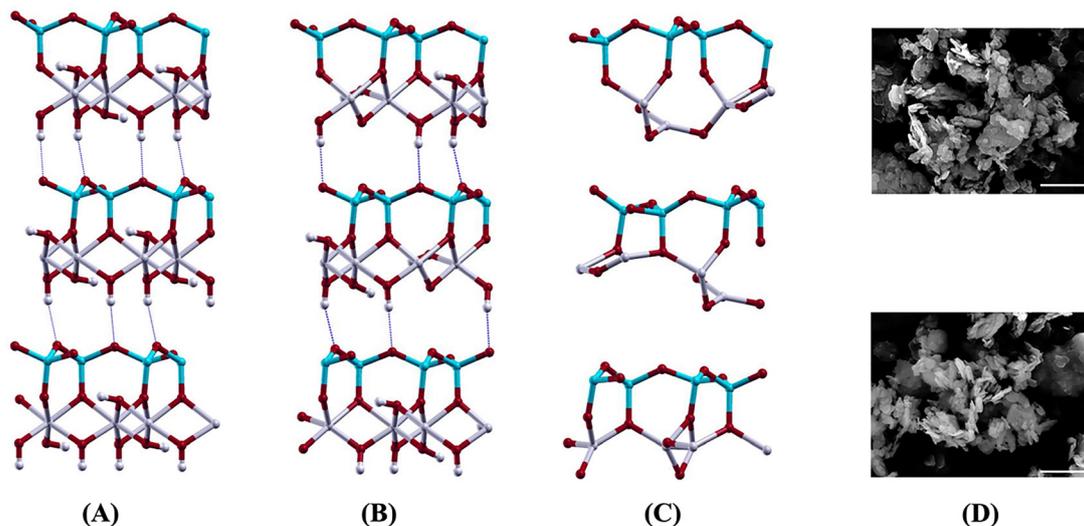
Fig. 2 (A) Disordered Kln ($Al_{12}Si_{12}O_{30}(OH)_{24}$), (B) partially dehydroxylated disordered Kln ($Al_{12}Si_{12}O_{33}(OH)_{18}$), (C) metadiskaolin ($Al_{12}Si_{12}O_{42}$), and (D) SEM images of disordered Kln KGa_2 (upper), and metadiskaolin KGa_2 615 C (lower);[114] reproduced from Izadifar et al., 2020,[114] licensed under CC BY 4.0.
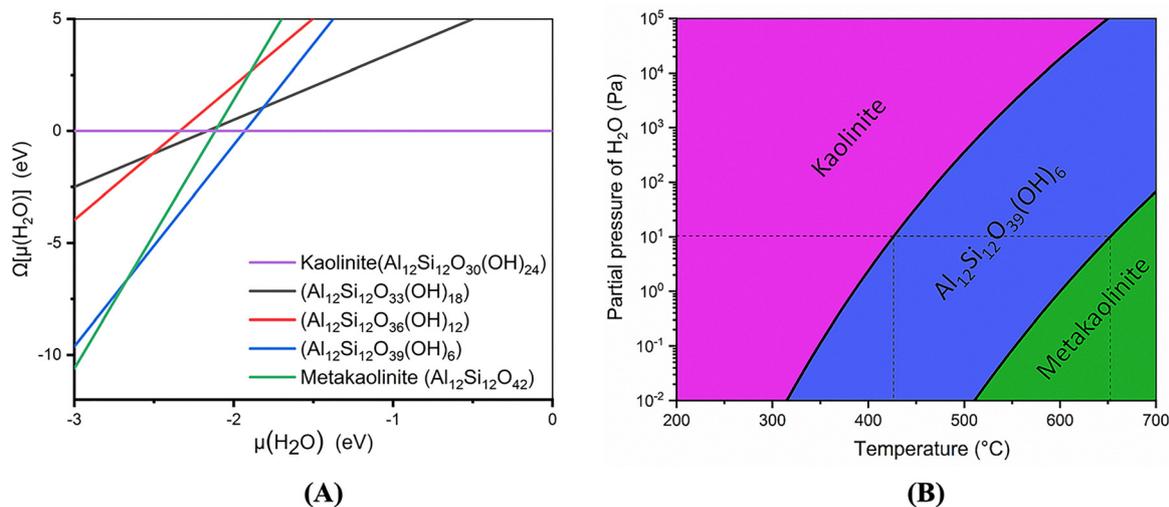

Fig. 3 (A) Phase diagram of Kln ($Al_{12}Si_{12}O_{30}(OH)_{24}$) to MK ($Al_{12}Si_{12}O_{42}$) transformation calculated, as a function of the water chemical potential (B) density-temperature (ρ,T)-phase diagram;[114] reproduced from Izadifar et al., 2020,[114] licensed under CC BY 4.0.

formation of stable $Al_{12}Si_{12}O_{33}(OH)_{18}$ phase during the initial stage of DHX.

It is also worth mentioning that Kln with disordered structure, often referred to as "low crystallinity" or "disordered Klns", tend to dehydroxylate at lower temperatures compared to those with more ordered structures.[114]

Changes in unit cell volume has been observed during the transformation of Kln to MK and disordered Kln to metadiskaolin.[114] By employing the Birch-Murnaghan diagram to analyze complete DHX at the equilibrium point,[129] they observed a notable expansion in the unit cells of both MK and metadiskaolinite, as depicted in Fig. 5. Their results demonstrated that the supercell of MK expanded by roughly 4%, whereas metadiskaolin expanded by

approximately 8%, compared to ordered and disordered Kln, respectively.[114]

3.2. Metakaolin dissolution and reactivity

The dissolution rate of pozzolanic materials is a critical determinant of their reactivity within cementitious systems. Generally, a higher dissolution rate enhances reactivity by promoting the release of reactive species essential for the formation of binding phases.[33] Studies have shown that MK dissolves rapidly in alkaline environments during the initial stages, releasing $(SiO_4)^{4-}$ and $Al(OH)_4^{-}$ reactive species. This early dissolution phase is often congruent, with reactive species released in proportions similar to their original concentrations in the material. However, over time, the dissolution rate tends to
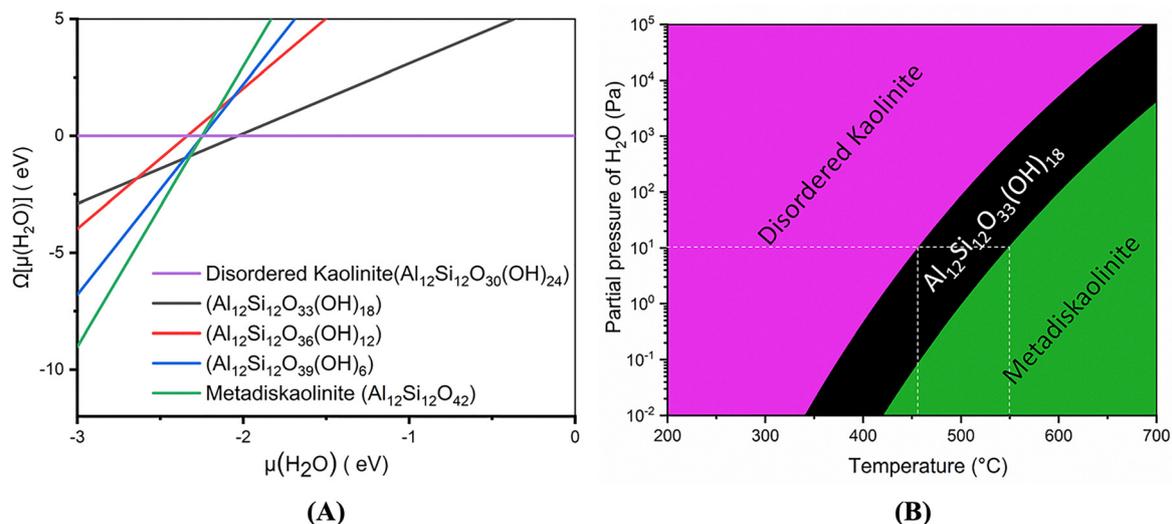
Fig. 4 (A) Phase diagram of disordered Kln ($Al_{12}Si_{12}O_{30}(OH)_{24}$) to metadiskaolin ($Al_{12}Si_{12}O_{42}$) transformation calculated, as a function of the water chemical potential (B) density–temperature (ρ,T)-phase diagram;[114] reproduced from Izadifar *et al.*, 2020,[114] licensed under CC BY 4.0.
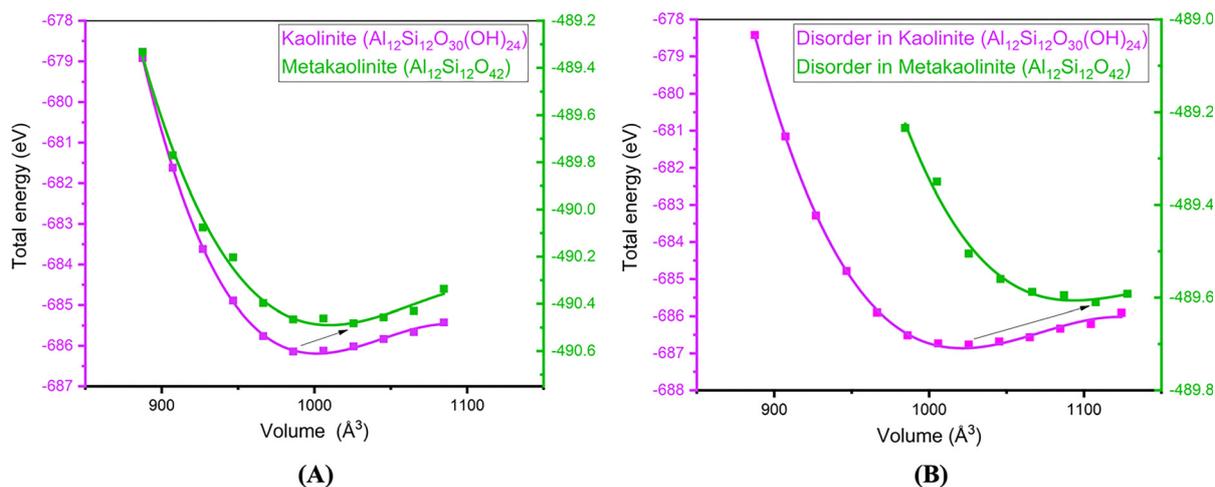

Fig. 5 Birch–Murnaghan diagram of (A) Kln to MK, (B) disordered Kln to metadiskaolin;[114] reproduced from Izadifar *et al.*, 2020,[114] licensed under CC BY 4.0.

slow, and the process may become incongruent, resulting in varied Si/Al ratios in the solution. This shift influences the availability of reactive species, thereby influencing the material's overall reactivity.[33,130]

The dissolution of MK is influenced by several factors, including pH levels,[22,33,130–132] alkali hydroxide concentration,[33,133,134] calcination temperature,[122,135–137] surface area,[138] Si/Al ratio,[23,33,122,131,138,139] and the type of activator used. Concerning pH, Beuntner *et al.*[22] reported that the dissolution of MK increases at higher pH levels, leading to enhanced reactivity within the system. Chen *et al.*[140] recently demonstrated that elevated alkalinity induces the exfoliation of MK particles, exposing interior surfaces to the alkaline solution and thereby facilitating the dissolution of bulk-like components. At high alkalinity, the exfoliation of MK particles exposes a greater

surface area to the solution, thereby increasing the apparent dissolution rate. Similarly, Scherb *et al.*[138] concluded that material's surface area influence ion adsorption, which subsequently affects the pore solution and, ultimately the dissolution and reaction behavior of the material. Weng *et al.*[132] observed that the dissolution of MK in alkaline environments is driven by the breakdown of covalent oxo-bridging between many $(SiO_4)^{4-}$, leading to the release of $(SiO_4)^{4-}$ and $Al(OH)_4^-$ ions into the solution. As alkalinity increases, $(SiO_4)^{4-}$ species become more dominant in the solution, further enhancing the material's dissolution and reactivity.[141] Extensive research has been carried out to evaluate the influence of calcination temperature on the solubility of MK. These studies consistently identify 700 °C as the optimal calcination temperature for achieving maximum solubility of MK.[122,135–137]
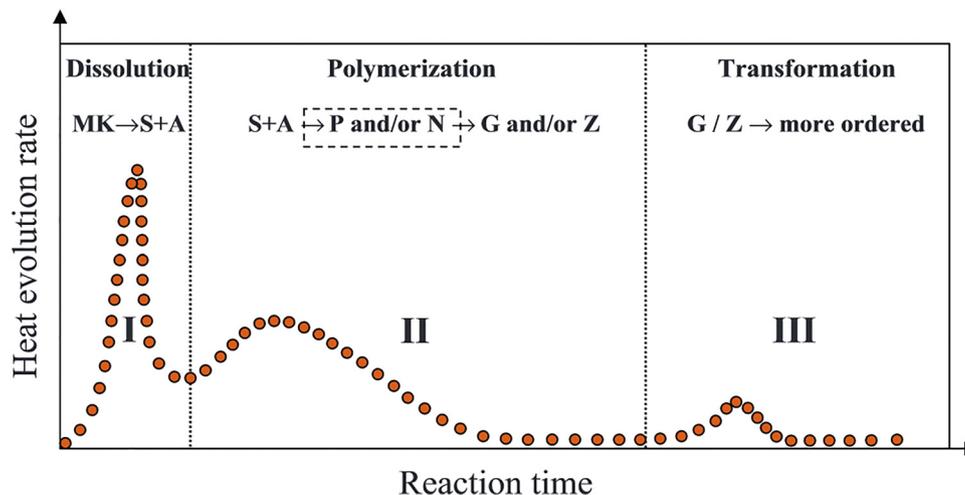
Fig. 6 Schematic representation of the kinetics of geopolymer synthesis *via* NaOH activation of MK, as analyzed through isothermal calorimetry. In this context, key abbreviations are defined as follows: MK, $(SiO_4)^{4-}$ monomers (S), $Al(OH)_4^-$ monomers (A), aluminosilicate oligomers (O), geopolymeric fragments (P), proto-zeolitic nuclei (Z), and aluminosilicate inorganic polymer gels (G).[30] Reproduced with permission from Elsevier Science & Technology Journals © 2012 (permission conveyed through Copyright Clearance Center, Inc.).[30]

The Si/Al ratio plays a crucial role in determining the dissolution of MK during geopolymerization. A higher Si/Al ratio can hinder the dissolution and release of precursor materials in an alkaline environment, resulting in unreacted MK particles in the final product.[139] While numerous studies have investigated the dissolution of MK at Si/Al ratios close to 1.0 in various alkaline solutions over extended durations,[33,131,138,142] Wang *et al.*[139] reported that increasing the Si/Al ratio to 1.95 can cause saturation during the dissolution process. This saturation ultimately has a negative impact on the compressive and flexural strength of the geopolymer. In this context, Garg *et al.*[122] highlighted a strong correlation between the rate of MK dissolution and the degree of undersaturation. Their findings showed that MK dissolves rapidly in the initial stage, but dissolution gradually slows down as the system approaches equilibrium. Additionally, they found that the Si/Al ratio in the solution is influenced by the calcination temperature used during MK production.

Fig. 6 from Provis[23] further demonstrated that the Si/Al ratio, along with calcium (Ca) and magnesium (Mg) content, plays a significant role in influencing phase formation and the degree of crystallinity in alkali-activated binders. It has been illustrated that the green and blue zones represent ordered and disordered phases, respectively. Systems with low Ca and/or Mg content typically form zeolites as the primary crystalline secondary products. In contrast, Mg-rich GGBFSs in blast furnace-slag-based binders with adequate Al content primarily produce hydrotalcite as the secondary crystalline phase. Alkaline activators play a crucial role in influencing the dissolution and reactivity of pozzolanic materials. This pivotal aspect will be explored in greater detail in the following section.

3.3. Effect of alkaline activator

Alkaline activators are key to enhancing the dissolution and reactivity of pozzolanic materials. This section reviews the dissolution and reactivity of MK in various alkaline solutions, such as NaOH, KOH, CH, KS. Furthermore, the impact of other critical parameters, such as activator concentration, temperature, and additional relevant factors, is thoroughly evaluated.

Alkali activators, typically solutions of NaOH or KOH, markedly accelerate the dissolution rate of MK.[11,23,143–145] The elevated alkalinity breaks down the amorphous aluminosilicate network in MK, promoting the release of reactive Si and Al ions.

The impact of NaOH on the dissolution and reactivity of MK lies in its ability to break down the aluminosilicate structure of MK, thereby facilitating the release of key reactive species, primarily Si and Al. MK, an amorphous aluminosilicate material, undergoes significant dissolution when exposed to an alkaline NaOH solution. The hydroxide ions (OH^-) provided by NaOH attack the aluminosilicate network, breaking Si–O–Si and Si–O–Al bonds within the MK structure.[73,146] This disruption by hydroxide ions is critical for dissolution, enabling the release of Si and Al ions into the solution.[130,140]

Zhang *et al.*[30] explored the kinetics of MK geopolymerization through reaction with NaOH solution at temperatures ranging from 20 to 40 °C, employing isothermal conduction calorimetry. They developed a diagram, illustrated in Fig. 6, that correlates three distinct exothermic peaks with the reaction stages of geopolymerization. This diagram builds upon reaction kinetics models of geopolymerization proposed by Provis *et al.*[147,148] The first peak corresponds to MK dissolution, marking the release of reactive components. The second peak represents the polymerization of dissolved species and their subsequent transformation into cross-linked or zeolitic structures. Finally, the third exothermic peak reflects further structural reorganization, stabilizing the material in a more durable, though not necessarily crystalline, state.[30]

Zhang *et al.*[30] further observed that increasing the NaOH concentration up to a molar Na/Al ratio of 1.1 significantly enhances the reaction extent over three days, achieving a
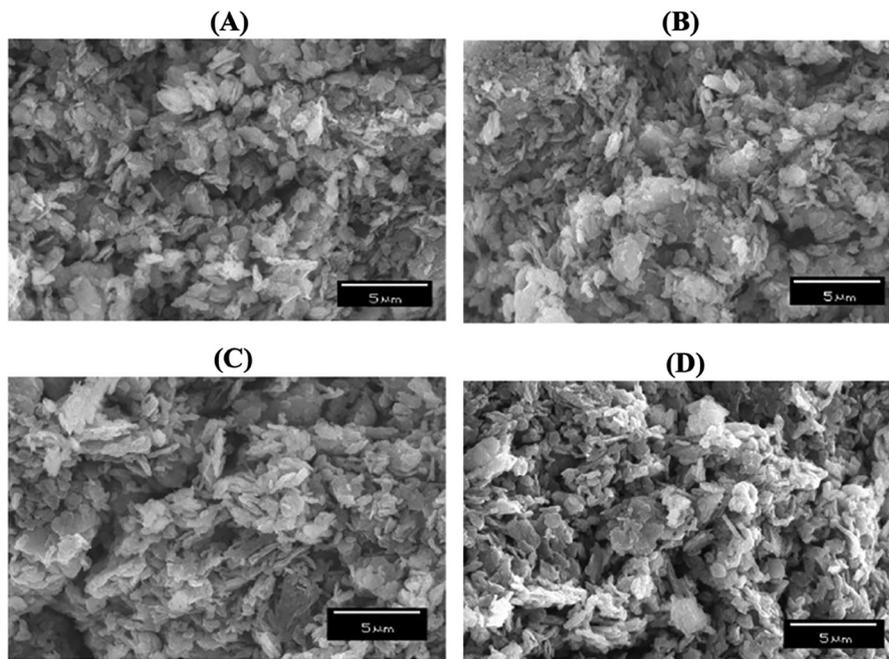
Fig. 7 SEM micrographs of the fracture surfaces of geopolymerization products of MK activated with NaOH solution at different concentrations: (a) 6 mol L^{-1}, (b) 8 mol L^{-1}, (c) 10 mol L^{-1}, and (d) 12 mol L^{-1}.[30] Reproduced with permission from Elsevier Science & Technology Journals © 2012 (permission conveyed through Copyright Clearance Center, Inc.).[30]

maximum degree of approximately 40% in high liquid-to-solid ratio systems. This increase also accelerates the crystallization process. However, further additions of NaOH beyond this concentration do not result in additional reaction progression or further acceleration during the same period.

Boonjaeng et al.[135] investigated the pozzolanic reaction of MK and CH under alkaline activation, focusing on the influence of NaOH concentration. Their findings revealed distinct reaction regimes depending on the NaOH concentration. At low NaOH concentrations (<1 M), the pozzolanic reaction dominated. As the concentration increased to a medium range (1 M < NaOH <5 M), zeolitic reactions became the primary process. At higher concentrations (> 5 M), geopolymerization emerged as the dominant reaction mechanism.

Zhang et al.[30] further noted that exposure of MK to highly concentrated NaOH solutions led to the transformation of MK particles into a porous, particulate gel. These gel particles adhered to one another, either along their surfaces or edges, while partially retaining the original plate-like morphology of MK, as evidenced by SEM imaging (Fig. 7). Duxson et al.[149] also reported the formation of porous gel morphologies in MK-based geopolymers with low Si/Al ratios.

Temperature also plays a critical role in the reaction kinetics. Raising the reaction temperature from 25 to 40 °C was found to accelerate the initial reaction rate. However, this increase in temperature had minimal impact on the final reaction extent, particularly when the Na/Al ratio exceeded 1.[30] Garg et al.[122] demonstrated that the solubility of MK in a 0.1 M NaOH solution was highest when the MK was calcined at 700 °C, compared to calcination temperatures of 500 and 900 °C.

Scherb et al.[33] examined the solubility of MK in various solutions, including deionized water, KOH, and NaOH. In their experiments, 5 grams of MK were mixed with 400 mL of each solution and agitated for 24 hours using a vibrating unit. The pH values of the solutions were measured as 5.8 for deionized water, 13.2 for 10 wt% NaOH, and 14.1 for 10 wt% KOH. The showed minimal weight loss of MK in deionized water (0.07 grams), while significantly higher losses were observed in alkaline solutions: 2.96 grams in NaOH and 1.25 grams in KOH. This indicates that NaOH caused the greatest dissolution among the tested solutions. Additionally, the concentrations of SiO_2 and Al_2O_3 increased in the alkali solutions, with NaOH showing a more pronounced effect, attributed to its enhanced ability to dissolve Si and Al ions. Garg et al.[122] measured the initial dissolution rate of MK in a 0.10 mol L^{-1} NaOH solution, and its long-term reaction behavior. During the first 24 hours under far-from-equilibrium (highly diluted) conditions, the initial dissolution rates for both Al and Si remained constant at 38 μmol L^{-1} h^{-1}. Beyond this period, as the system approached equilibrium, the dissolution rate decreased, highlighting the importance of differentiating the fundamental roles of forward and reverse dissolution reactions from other precipitation processes. Werling et al.[150] focused on the phases formed during geopolymerization by the solubility of MK and amorphous SiO_2 in NaOH solutions at various concentrations. Their findings revealed that the solubility of MK, calcined at 700 °C increased with rising NaOH concentrations. In lower NaOH concentrations (0.01 and 0.1 mol L^{-1}), Si solubility remained below 5% even after 24 hours and 7 days. However, in a 10.79 mol L^{-1} NaOH solution, Si solubility in MK increased significantly, reaching 65% after 24 hours and 80% after 7 days.
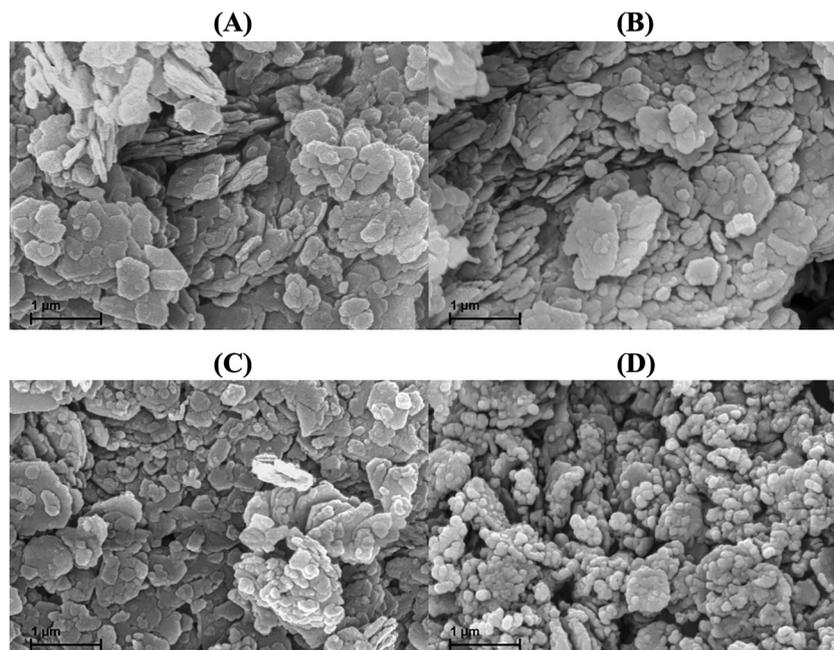
Fig. 8 SEM images of gold-coated samples: (A) MK; (B) MK mixed with water; (C) MK treated with KOH; (D) MK treated with NaOH;[33] reproduced from Scherb et al., 2020,[33] licensed under CC BY 4.0.

Scherb et al.[33] also utilized SEM to analyze the solubility of MK in deionized water, KOH, and NaOH, as shown in Fig. 8. The SEM images revealed significant microstructural changes in the MK-NaOH solution, including alterations in particle morphology and size reduction. These changes are attributed to the dissolution of Si and Al monomers, which reshape the particles. Palomo et al.[151] further emphasized that the dissolution of aluminosilicates in high-pH environments facilitates the release of Si- and Al-monomers.

Hajimohammadi et al.[133] analyzed MK dissolution in NaOH solutions and observed only a slight increase in the maximum concentrations of Al and Si ions in solution when NaOH concentration was raised from 0.05 M to 0.3 M. Wang et al.[152] investigated geopolymers with varying MK contents activated by a mixed alkaline solution of NaOH. They found that increasing the MK proportion resulted in a more porous structure, which negatively impacted the overall quality and performance of the geopolymers. Granizo et al.[130] examined the effect of CH addition on the alkali activation of MK in NaOH solutions at different concentrations. Their results showed that a 12 M NaOH solution was required for complete MK activation and network structure formation. However, the addition of CH promoted C–S–H gel formation even at lower NaOH concentrations. Despite this advantage, CH hindered alkali-network structure development by reducing ion mobility at higher pH level. Comparing NaOH with KOH, Panagiotopoulou et al.[131] studied the leaching behavior of aluminosilicate minerals, including kaolin, MK, FA, and GGBFS, in these alkaline solutions. They found that NaOH was more effective than KOH in dissolving aluminosilicates, particularly for highly reactive materials. Notably, the leaching of Si and Al was synchronized in both solutions, with this behavior being more pronounced in

kaolin and MK, which consist predominantly of a single aluminosilicate phase. Gharzouni et al.[153] examined the effects of MK reactivity and alkaline solution composition on geopolymer formation. Using four different MKs and two KS solutions with varying pre-reacted components, they demonstrated that MK reactivity predominantly controls network formation and strength when using less reactive alkaline solution. Conversely, in highly reactive alkaline solutions, the pre-reacted components dictate geopolymerization and performance, regardless of the MK used. These findings suggest that tailoring the reactivity of both MK and KS solutions enables precise customization of geopolymer properties through thoughtful component selection.

In another study, Gharzouni et al.[154] examined how varying potassium-activating solutions affected MK reactivity. They found that the initial Si/K molar ratio of the $(SiO_4)^{4-}$ solution significantly influenced the type and concentration of siliceous species. Lower Si/K ratios led to greater depolymerization, producing smaller and more reactive entities. These reactive species facilitated Si bridging, promoting rapid oligomer formation and enhancing the mechanical properties of the resulting geopolymersexamined how varying potassium-activating solutions affected MK reactivity. They found that the initial Si/K molar ratio of the $(SiO_4)^{4-}$ solution significantly influenced the type and concentration of siliceous species. Lower Si/K ratios led to greater depolymerization, producing smaller and more reactive entities. These reactive species facilitated Si bridging, promoting rapid oligomer formation and enhancing the mechanical properties of the resulting geopolymers.

Tippayasam et al.[155] explored the use of potassium-based alkali solutions (KOH and KS) in geopolymer production. They identified optimal conditions for MK based geopolymers: 10 M

Table 4 Kaolinite and metakaolin-Priority research topic & key question

Topics	Key research questions to be solved
Structural transformation of kaolinite to order- disorder MK	How do heating conditions, morphology, and stacking order affect dehydroxylation and MK reactivity?
Aluminum coordination and short-range order	How does Al coordination (IV, V, VI) influence dissolution, and can calcination optimize it?
Dissolution behavior and controlling factors	How do pH, activator type/concentration, calcination temperature, surface area, and Si/Al ratio affect MK dissolution?
Influence of alkaline activators	How do NaOH, KOH, KS, and CH differ in dissolution mechanisms, gel formation, and optimal activation?

KOH, curing at 40 °C for 24 hours, followed by heat treatment at 550 °C. Heat treatment enhanced compressive strength but increased porosity due to water loss. The resulting microstructure displayed a more mature, ceramic-like quality, contributing to improved strength.

Beuntner et al.[156] investigated the dissolution kinetics of MK in alkaline solutions with varying alkalinity levels, including CH (pH 12.75), MOH1 (pH 13.57), MOH2 (pH 13.72), and KOH (pH 14.00). They found that the rate of MK solubility varied depending on the alkalinity of the solution. Solutions with higher alkalinity, such as KOH, exhibited faster dissolution rates. After 6 hours, a significant amount of dissolved Si and Al ions were observed due to the reactive $Al(OH)_4^-$ content of MK, with approximately 40% of the total solubility being leached within this time. Alventosa et al.[157] examined the influence of CH on alkali-activated MK pastes using a range of analytical techniques. Their findings revealed that CH has minimal effect on NaOH-activated systems but exerts a significant influence on Na_2SiO_3-activated systems, particularly at a concentration of 5 M. In NaOH-activated pastes, the common ion effect inhibits MK dissolution and delays the formation of N–A–S–(H) gel. Conversely, in 5 M Na_2SiO_3-activated pastes, the addition of CH accelerates N–A–S–(H) gel formation through the initial production of C–A–S–H gel, which enhances MK dissolution and raises the overall pH. These results suggest that incorporating CH into Na_2SiO_3-activated MK systems could reduce the required activator concentration.

Weise et al.[158] investigated the effects of CH availability and alkali activator type on the pozzolanic reactions of MK. They observed that higher MK/CH ratios, combined with the addition of alkali hydroxides (KOH and NaOH), accelerated MK dissolution and increased the Si/Ca and Al/Ca ratios in the resulting C–A–S–H gels. Significantly, KOH produced higher pH levels and faster reactions kinetics than NaOH. However, the overall acceleration of pozzolanic reactions was more pronounced with NaOH than with KOH, highlighting the differing influences of alkali hydroxides on the reactivity of MK. Key topics, along with research gaps and outstanding questions in this area, are summarized in Table 4.

4. Slag and fly ash

4.1. Slag and fly ash structures

GGBFS and FA are two widely used pozzolanic materials in cementitious systems, valued for enhancing concrete durability

and reducing the environmental footprint of traditional cement. Both possess aluminosilicate-based compositions that enable reactions with CH during hydration, leading to the formation of additional cementitious phases. Despite differences in composition and reactivity rates, GGBFS and FA exhibit comparable dissolution mechanisms, making them complementary in blended cement formulations.

GGBFS is a byproduct of the ironmaking process, produced by rapidly quenching molten slag with water and then grinding it into a fine powder. It is a significant solid waste in the ferrous metallurgical industry and has a unique $(SiO_4)^{4-}$ structure. Its composition dominated by CaO, SiO_2, Al_2O_3, and magnesium oxide (MgO, M).[159,160] In its ground granulated form, (GGBFS) is widely used as a pozzolanic material in cementitious systems due to its ability to enhance concrete durability, reduce the heat of hydration, and contribute to lower CO_2 emissions.[161–163] The C–A–S–H composition of GGBFS enables it to react with CH generated during cement hydration, forming additional C–S–H phases that improve the density and strength of concrete. Studies have shown that partial replacement of PC with GGBFS (up to 50%) enhances resistance to chloride ion penetration, thereby reducing corrosion risks in reinforced concrete, especially in marine environments.[161] The crystal structure of GGBFS plays a critical role in its pozzolanic reactivity and suitability for cementitious applications. GGBFS primarily consists of C–A–S–H phases that can form various crystalline structures depending on cooling conditions and chemical composition. Rapid cooling yields an amorphous, glassy phase with a depolymerized network of SiO_4 and AlO_4 tetrahedra, stabilized by interstitial cations such as Ca^{2+} and Mg^{2+}.[164] In contrast, slower cooling leads to the formation of crystalline phases such as gehlenite, akermanite, and merwinite, with distinct columnar or plate-like morphologies at various temperature ranges.[165] The phase composition and structure are strongly influenced by the CaO/SiO_2 ratio, as well as the contents of MgO, and Al_2O_3. For instance, higher CaO/SiO_2 ratios reduce the degree of polymerization in the GGBFS, leading the formation of crystalline phases such as merwinite and gehlenite during cooling process.[166] Variations in Al_2O_3 and MgO content also influence the crystal structure; increased Al_2O_3 promotes greater polymerization and alters the onset temperature of crystallization.[167] Analytical techniques such as differential scanning calorimetry (DSC) and Raman spectroscopy have revealed that, as Al_2O_3 content increases, the dominant crystalline phases shift from silicate-based $(SiO_4)^{4-}$ networks to aluminate-based structures.[168]

FA[169,170] is also a key source material for geopolymer production, composed of finely divided ashes produced from the combustion of pulverized coal in thermal power plants. Its chemical composition varies based on the mineralogy of the parent coal, with typical SiO_2 content ranging from 40% to 60% and Al_2O_3 content between 20% and 30%. The iron content in FA can vary significantly, and notable quantities of alkalis are present, with potassium typically more abundant than sodium.[171] Its structural and chemical composition, primarily aluminosilicates and SiO_2, makes FA an effective pozzolanic material in the cement industry. During hydration, FA reacts with CH through a pozzolanic reaction, forming C–S–H and other phases such as calcium aluminate hydrate (C–A–H), C–A–S–H, which contribute to improved concrete strength and durability.[172] FA has been shown to effectively replace up to 30% of PC, leading to improved workability, reduced heat of hydration, and enhanced long-term strength in a wide range of concrete applications.[173] Additionally, FA is highly effective in high-performance concrete formulations for 3D-printed structures and eco-friendly applications, significantly reducing the environmental footprint associated with traditional cement production.[174] Further studies have confirm that incorporating low-Ca FA into cement systems enhances mechanical strength and durability, particularly under high-pH or alkali-activated conditions that optimize its reactivity.[175–177] FA's performance can be further enhanced by reducing particle size, which increases surface area and accelerates early-stage reactions in blended cements.[178] Its use as a SCM supports sustainable construction by lowering CO_2 emissions and conserving natural resources.[179] Fernandez-Jimenez et al.[146] reported that the fineness of FA significantly influences the development of mechanical strength in materials produced after activation. Additionally, the surface charge on FA particles affects the initial setting properties of geopolymeric mixtures, as the early transport of hydroxyl ions to the particle surface plays a crucial role in initiating the setting process.[29]

As shown in Fig. 9, when raw materials rich in Si and Al, such as GGBFS and FA, are activated by an alkaline solution, the dissolved AlO_4 and SiO_4 tetrahedra bond through shared oxygen atoms, resulting in the formation of monomers. These monomers then interact to generate oligomers, which subsequently undergo polymerization, resulting in the formation of a 3D network of aluminosilicate structures.[180,181] The resulting alkali-activated aluminosilicates exhibit remarkable properties, including high strength, enhanced durability, and strong resistance to chemical degradation.[76,180,182]

Lu et al.[183] compared the amorphous characteristics and morphologies of FA and GGBFS using scanning electron microscopy analysis. They found that FA primarily consists of spherical particles, including solid spheres and hollow cenospheres, formed by the rapid cooling of molten mineral matter during coal combustion. These particles exhibited smooth surfaces and variable sizes, with their amorphous glassy phases contributing significantly to their pozzolanic reactivity. In contrast, GGBFS particles are angular and irregular, with rough surfaces formed by the rapid quenching of molten iron slag during its
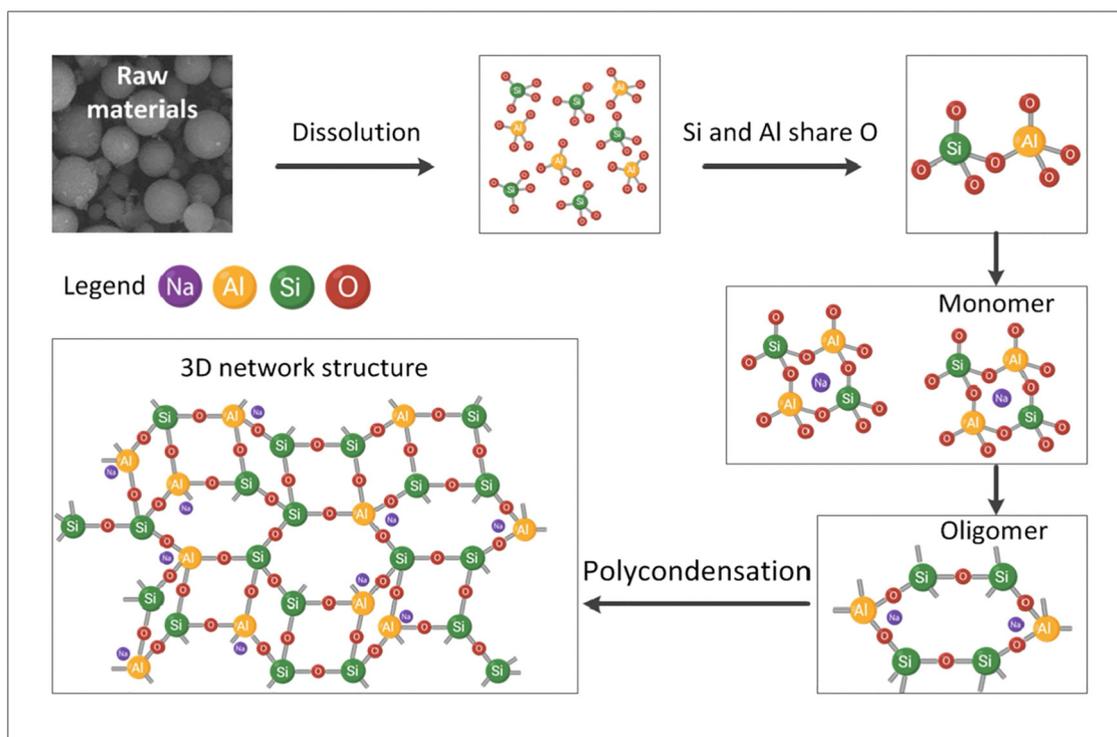

Fig. 9   Schematic of geopolymerization of GGBFS and FA.[182] Reproduced with permission from Elsevier Science & Technology Journals © 2020 (permission conveyed through Copyright Clearance Center, Inc.)[182]

production. This process prevented the formation of crystalline structures, making GGBFS predominantly amorphous and enhancing its latent hydraulic properties. The distinct morphologies and amorphous contents of FA and GGBFS significantly influence their respective reactivities and roles in cementitious systems.

4.2. Dissolution and reactivity of slag and fly ash

Alkali-activated GGBFS binders are synthesized through the chemical reaction of SiO_2 with an alkaline activator.[184] The properties of these binders are influenced by several key factors, including the chemical composition and mineralogy of the GGBFS,[185,186] particle size,[187,188] degree of amorphicity, and the type and concentration of the alkaline activator.[52,189,190] Curing conditions, such as relative humidity, temperature, and curing duration, also play a crucial role in determining the binder performance.[191] Among these factors, the chemistry of GGBFSs as well as the nature of activator are particularly significant, as they strongly influence both the mechanical properties of the resulting cement and its environmental impact.[11,189,192,193]

The chemistry of the GGBFS source plays a critical role in governing the reaction kinetics and the structural evolution of solid phases in alkali $(SiO_4)^{4-}$ activated binders. The composition of GGBFS directly influences the rate of reaction and determines the nature of the solid phases formed during hydration.[194] Ben Haha et al.[185] investigated the effect of MgO content using two alkaline activators, NaOH and sodium silicate solution ($Na_2SiO_3 \cdot 5H_2O$, commonly known as water glass, NS). They observed that higher MgO content in GGBFS accelerated the reaction process and enhanced early-age compressive strength. Specifically, increasing the MgO content from 8% to 13% promoted hydrotalcite formation and reduced Al uptake by C–S–H, resulting in a 9% increase hydrate volume and a 50–80% improvement in compressive strength after 28 days or more in water glass-activated GGBFS pastes. Over longer curing periods, MgO content primarily influenced the quantity of hydrotalcite-like phases.

Bernal et al.[194] further demonstrated that MgO in GGBFS-based alkali-activated binders affects the formation of secondary phases like zeolites and hydrotalcite. High MgO content favors hydrotalcite formation, whereas low MgO promotes the formation of zeolites. While low MgO levels (<7.5 wt%) can accelerate early-stage reactions, they may limit the extent of overall reaction and increase Al uptake in C–A–S–H products. Additionally, high MgO (>5 wt%) can reduce the Al/Si ratio in the final strucure due to greater Al incorporation into hydrotalcite formation.

In several studies, GGBFSs with relatively high Al_2O_3 contents (11–28 wt%) were activated using a combination of clinker and gypsum, anhydrite, lime, or plaster of Paris, with or without additional alkaline activators. These investigations explored how the Al_2O_3 content influences the reactivity of GGBFS and the mechanical properties of the resulting binder systems.[195–200]

Ben Haha et al.[186] investigated the effect of Al_2O_3 content in alkaline activators and found that, although Al_2O_3 altered the composition of the hydrate assemblage, it had little impact on the total hydrate volume or the compressive strength of alkali-activated GGBFS binders. Gruskovnjak et al.[201] studied super-sulphated GGBFS activated with 15 wt% $CaSO_4$ and 0.5 wt% KOH, demonstrating that GGBFSs with higher Al_2O_3 content exhibited increased reactivity during the first week, resulting in higher early compressive strength. Kucharczyk et al.[202] examined the influence of Al_2O_3 on GGBFS reaction kinetics and observed that increasing Al_2O_3 content from 8% to 12% significantly accelerated the reaction, while a further increase to 16% produced only a minor additional effect on the kinetics.

Jamil et al.[203] evaluated geopolymer composites made with potassium and GGBFS, observing that different heating conditions altered the composite structures. They also assessed the impact of GGBFS composition on phase transitions, finding that the presence of Si, Al, Ca, and Mg oxides accelerated the phase transition process.

Liu et al.[204] investigated the incorporation of high-alkali red mud with NaOH as an activator for GGBFS hydration, and found that increased alkalinity enhanced mineral activation, leading in shorter induction periods and accelerated hydration rates. They also observed that a higher NaOH concentration further accelerated hydration and reduced induction time; however, excessive alkali levels caused microstructural defects, which ultimately decreased the specimen's strength.

The performance of FA as a SCM in concrete is strongly influenced by its reactivity and dissolution rate. Extensive research has focused on identifying the key parameters controlling these characteristics, including chemical composition, particle size distribution,[178,205,206] environmental conditions,[207,208] glassy phase content,[209] methods of alkaline activation,[23,210] and the water-to-binder ratio.[211] Together, these factors govern the release of reactive species such as SiO_2 and Al_2O_3, which are essential to the pozzolanic and cementitious behavior of FA in concrete applications.

Key reactive components in FA are aluminosilicate glasses, which are characterized by their degree of polymerization. This degree of polymerization is determined by the ratio of network-modifying ions (like Ca^{2+}, Na^+, and K^+) to network-forming ions (Si^{4+} and Al^{3+}). Lower degrees of polymerization, indicated by higher ratios of network-modifying ions, generally lead to higher reactivity.[212,213] Studies employing synthetic C–A–S–H affirm the impact of composition, showing that different glass phases such as silicate-rich and Ca-rich aluminosilicates, exhibit varying reactivities. SEM-energy dispersive X-ray spectroscopy (EDS) and dissolution experiments demonstrated that these differences closely correlate with trends in depolymerization.[209,214,215] Advanced techniques such as nuclear magnetic resonance (NMR) have revealed that calcium's key role in depolymerization and reactivity enhancement, while Al primarily serves as a network former. Studies on $CaO–Al_2O_3–SiO_2$ glasses showed that increased Ca content significantly boosts reactivity, whereas Al's effect is less pronounced, likely due to its limited contribution to

depolymerization. These findings highlight the importance of precise phase characterization in optimizing FA as a SCM.[216] Aughenbaugh et al.[217] investigated the impact of glassy phases on FA reactivity, finding that high-Ca aluminosilicate glass exhibited the highest reactivity, followed by low- and medium-Ca glasses. Alkali-modified aluminosilicate glasses were more reactive than Ca-based ones, indicating that glass composition strongly influences reactivity, and Ca content alone is not a reliable predictor.

FA reactivity is influenced by particle size, with finer fractions generally exhibiting higher reactivity, as evidenced by increased heat release in both direct reactivity tests and cementitious pastes. Wang et al.[205] explored the particle size by fractionating five Class C and Class F FAs into three size ranges: below 20 μm, below 45 μm, and above 45 μm. Finer fractions exhibited higher reactivity, reflected in increased heat release during reactivity tests and cement hydration. Compositionally, finer Class C particles contained higher Ca contribution, further enhancing reactivity, whereas coarser particles resembled Class F ash. These findings highlight that size reduction enhances performance, though the effect is composition-dependent. Snellings et al.[178] examined the effect of size classification and milling on the siliceous FA reactivity, finding that fine classified and milled FAs exhibited 40–57% higher reactivity in the R3 heat release test compared to the original ash. Particle size had the greatest impact with finer ashes improving hydration kinetics, increasing portlandite consumption and promoting greater C–S–H formation.

As the impact of temperature, Wang et al.[207] demonstrated that temperature significantly enhanced FA dissolution and reactivity by accelerating chemical reactions and reducing surface gel barriers that hinder Si and Al leaching. This effect was amplified in the presence of alkali and sulfate (S) solutions, where S ions modify surface gel properties to promote more efficient dissolution. The process is governed by internal diffusion, underscoring its importance for optimizing FA performance in alkali-S cementitious systems. Kuenzel and Ranjbar[208] demonstrated that temperature significantly enhances the FA dissolution by increasing kinetic energy, facilitating more efficient bond breaking of solute molecules. At elevated temperatures like 145 °C, nearly all amorphous, highly reactive FA components dissolved within 2 hours, whereas lower temperatures like 65 °C required much longer to achieve similar dissolution. Time was also critical, with dissolution of reactive amorphous materials typically occurring between 2 and 24 hours, depending on the curing conditions.

4.3. The impact of alkaline activators

Several studies have investigated the influence of activators on GGBFS dissolution kinetics.[185,186,190,218–225] Among alkaline activators, NaOH, NS, and Na_2CO_3 are the most commonly used in alkali-activated material production.[11,226]

It has been observed that NaOH activation leads to a faster initial reaction than NS (water glass) activation in GGBFS-based systems. Ben Haha et al.[185] reported that higher MgO content in NaOH-activated GGBFS slightly increased degree of reaction,

boosting early hydration performance. Briki et al.[227] observed that the GGBFS reaction slowed during both early and late stages; within the first 30 minutes of the GGBFS-NaOH solution reaction, a nonsteady dissolution phase for Al, Si, and sulfur ions occurred, followed by a steady dissolution. Later, Al and Si release rates declined due to precipitation, initially matching but diverging after two days. The reactivity of GGBFS in NaOH solution was found to be six times higher than in cement paste after one day, with the slower reaction in cement paste attributed to the presence of Ca ions from clinker phases. Yan et al.[228] investigated the reactivity of GGBFS in NaOH solutions and found that the dissolution rates of Si and Al ions were significantly influenced by the combined effects of NaOH concentration and temperature. These ions facilitated the formation of N–(C)–A–S–H gels, which are critical in alkali-activated cement systems. Their study demonstrated that the leaching process was governed by surface chemical reactions on unreacted particles, with maximum dissolution occurring under higher NaOH concentrations and elevated temperatures. Ravikumar et al.[229] studied the effect of activator type (powder NS vs. water glass) on the early-age reaction kinetics of alkali-activated GGBFS pastes. They found that powder NS-activated GGBFS pastes behave similarly to NaOH-activated GGBFS, with a single early-age reaction peak. Water glass-activated GGBFS pastes, however, exhibited a response similar to ordinary Portland cement (OPC) pastes, with a distinct induction period. Na_2CO_3-activated GGBFS pastes typically take significantly longer to set compared to those activated with NS or NaOH.[218,219,230,231] The prolonged hardening in alkali-activated slag (AAS) is due to the slow rise in alkalinity needed to initiate GGBFS dissolution. In other words, Ca ions from dissolved GGBFS reacts with carbonate from the activator to form salts like calcite, which releases hydroxide ions and raises pH. However, $(SiO_4)^{4-}$ dissolution is not rapid, as Na_2CO_3 activators have a pH is below 12.[219,230] Bernal et al.[230] examined the hydration process of GGBFS activated with Na_2CO_3 and observed an extended induction period of 3–5 days in some systems. They suggested that the CO_3^{2-} functional group in the activator promoted the formation of calcium carbonate (Cc) before the precipitation of C–A–S–H. Additionally, the lower pH of the carbonate compared to NS was found to delay the initial reaction rate of the GGBFS. Ke et al.[192] investigated the effects of calcined layered double hydroxide (CLDH) on Na_2CO_3-activated GGBFS cements and found that CLDH significantly accelerates the reaction and hardening process. The MgO content in the GGBFS also influences the reaction kinetics. CLDH's effectiveness is attributed to its ability to remove dissolved CO_3^{2-} and increase pH. They highlighted that the activator's functional group is the primary factor controlling reaction kinetics. Gebregziabher et al.[232] compared the effects of activator on the hydration of AAS at different temperatures. They found that NaOH-activated GGBFS hydrates much faster than NS-activated GGBFS. SiO_2 in the activator retards hydration in NS-activated GGBFS but can lead to denser products and higher later-age strength. They also found that elevated temperature curing can accelerate product formation and strength

gain in NS-activated GGBFS, although it may also lead to microcracking.Fernandez-Jimenez et al.[233] conducted a study on the early stages of alkaline activation in GGBFS. They used calorimetry to measure the reaction process and analysed the effects of different alkaline activators, including NaOH, water glass (NS) with NaOH, and Na_2CO_3. The results showed that the reaction mechanism shifts at certain points during the process, with diffusion playing a key role in the advanced stages. They concluded that the nature of the alkaline activator influences the degree of hydration and the kinetics of the reaction, indicating variability based on the activator used.

As for FA, Wang et al.[207] demonstrated that the dissolution process of FA is governed by internal diffusion in alkali and alkali-S solutions. The study revealed that the synergistic effect of alkali and S significantly enhanced the dissolution concentrations of Si and Al, particularly when the solution contained 5 mol L^{-1} NaOH and 0.01 mol L^{-1} Na_2SO_4. Furthermore, S ions (SO_4^{2-}) promoted additional dissolution of FA particles by altering the gel properties on their surface in the alkaline environment, facilitating greater reactivity.

Kuenzel and Ranjbar[208] found that the concentration of the alkaline solution, specifically NaOH within the range of 8–16 M, had a relatively limited impact on the dissolution of FA under the experimental conditions. The high liquid-to-solid ratio ensured that sufficient hydroxide ions were available for reaction, with NaOH primarily maintaining the alkaline environment necessary for the dissolution process. While the solution's molarity had minimal effect on the dissolution rate, it ensured the stability of dissolved species and facilitated the breakdown of reactive amorphous aluminosilicates. The findings emphasized that beyond providing the necessary pH, increasing NaOH concentration did not significantly enhance reactivity under high liquid-to-solid ratio systems. According to,[234] the dissolution of FA in alkaline CH solutions was analyzed over 48 hours. FA exhibited pozzolanic activity in both 1 mol L^{-1} and 0.1 mol L^{-1} solutions. The concentration of active ions (Al^{3+}, Fe^{3+}, and Si^{4+}) fluctuated with time, with Al^{3+} and Si^{4+} ions peaking at 6 and 24 hours, while Fe^{3+} ions decreased. The conductivity of the solutions declined over time, with a stronger pozzolanic reaction observed in the 1 mol.L^{-1} solution compared to the 0.1 mol L^{-1} solution. Microscopic analysis showed an increase in long, slender products as dissolution progressed. A study by Chen et al.[235] investigated the dissolution and reactivity of FA in KOH solutions, revealing three distinct stages. In the first stage ($\alpha < 0.1$, where α represents the relative mass of FA reacted), dissolution was controlled by glass network dissolution, with minimal gel formation. In the second stage ($0.1 < \alpha < 0.45$), a thicker gel formed from Fe, Ca, Mg, and Ti oxides, and dissolution became diffusion-limited. In the third stage ($\alpha > 0.45$), zeolite crystallized over the gel, and aluminosilicate gel formed. The study showed that the rate constant in the first stage increased with the concentration of network formers, highlighting the role of chemical durability, while in the second stage, the rate constant increased with OH^- concentration, indicating OH^- ions as the rate-limiting factor. Wilinska and Pacewska[236] investigated the

influence of KOH concentration on the hydration processes of different FAs. They found that in 0.1 M KOH solutions, fluidized FA reacted to form AFt, while conventional FA exhibited minimal reaction. At higher concentrations (4 M KOH), hydration occurred in both types of FA, with conventional FA forming an amorphous aluminosilicate gel and fluidized FA producing zeolitic products, particularly at elevated temperatures during early hydration.

Glosser et al.[237] developed a standardized method to assess FA reactivity, combining CH and FA with exposure to KOH solution. Reactivity, ranging from 33% to 75%, was measured through isothermal titration calorimetry (ITC), thermogravimetric analysis (TGA), and thermodynamic modeling. The results showed that FA reactivity significantly impacts durability-related properties such as CH content, C–S–H formation. Fernandez-Jimenez's study[220] demonstrated the different dissolution rates and reactivity of NaOH, Na_2CO_3, and NS (water glass) in alkali-activated FA binders. It was observed that NaOH accelerated early strength gain, NS improved long-term strength, and Na_2CO_3 modified the microstructure for better durability. NaOH exhibited the highest reactivity due to its high OH^- concentration, leading to rapid dissolution of FA and early formation of an aluminosilicate gel with a low Si/Al ratio (1.6–1.8) contributing to fast strength development. NS, though slower to dissolve, produced a gel with higher SiO_2 content, enhancing compressive strength over time. Na_2CO_3 had the slowest dissolution rate and promoted the formation of secondary crystalline phases like zeolites, which influenced long-term durability.

The impacts of activator characteristics and temperature on the dissolution behavior and reactivity of FA in alkali-activated systems were assessed by Palacios et al.[238] They compared NaOH and NS (waterglass) as activators. At room temperature, pastes activated with NS exhibited lower yield stress than those activated with NaOH. This reduction in yield stress was attributed to the adsorption of silicates from the NS solution, which increased the negative surface charge on FA particles, enhancing interparticle repulsion and leading to particle deflocculation. Elevated temperatures and higher concentrations of the alkaline solution led to increased yield stress, linked to heightened FA reactivity and greater formation of early hydration products.

A study by Deir et al.[239] investigated the influence of starting material (S, class C FA with higher Ca content, and class F FA with lower Ca content) on the hydration kinetics and gel composition in alkali-activated binder systems. The results showed that class C FA pastes had the highest initial reaction peak in calorimetry tests, followed by GGBFS and class F FA pastes (Fig. 10). Cumulative heat evolved correlated with compressive strength, with GGBFS mixtures releasing more heat than C-FA mixtures.

Deng et al.[240] compared the reactivity of FA and GGBFS in various alkaline environments, focusing on Al dissolution and product formation. They observed that while FA contains significantly more Al_2O_3 than GGBFS, its reactivity is much lower, resulting in fewer Al-containing products. In FA-CH
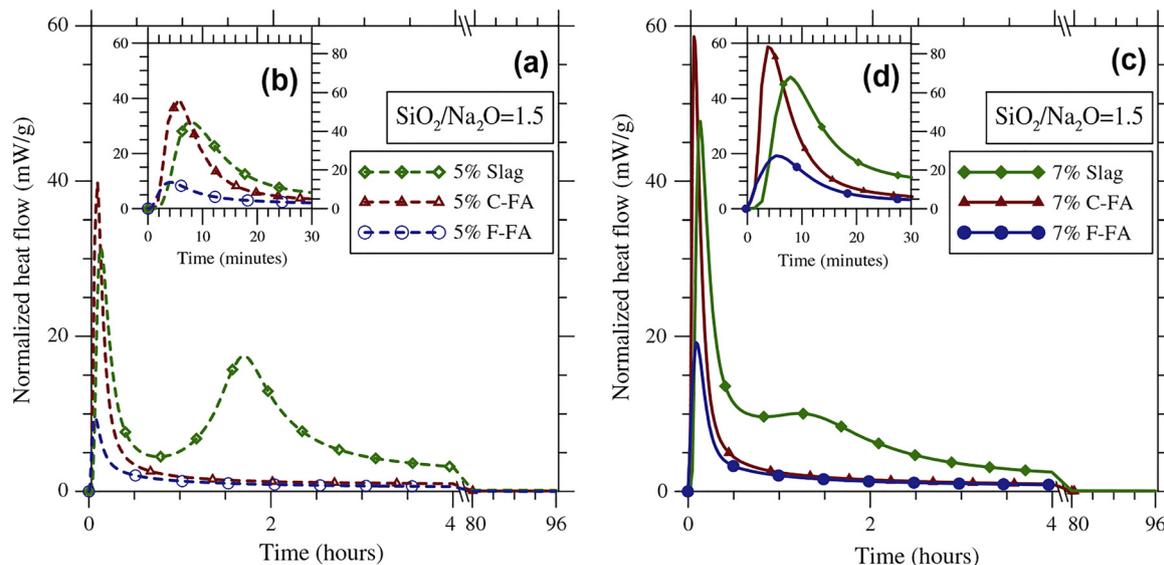
Fig. 10 Normalized heat flow for alkali-activated pastes made from different starting materials and activated with (a) and (b) 5 wt% Na$_2$O and (c) and (d) 7 wt% Na$_2$O solutions, measured using isothermal conduction calorimetry at 50 °C.[239] Reproduced with permission from Elsevier Science & Technology Journals © 2014 (permission conveyed through Copyright Clearance Center, Inc.).[239]

systems, Al primarily formed tetra-clcium aluminate hydrate (CAH$_{13}$, C$_4$AH$_{13}$), C–A–S–H, and minor monosulfoaluminate (Ms, C$_4$AsH$_{12}$), with sulfates promoting Aft formation and reducing Al incorporation into C–S–H. Conversely, in GGBFS-CH systems, Al was predominantly incorporated into hydrotalcite (HT), TAH, and C–A–S–H, with sulfates facilitating the migration of Al from TAH and C–A–S–H to AFt and Ms. GGBFS pastes consistently exhibited higher ratios of Al(VI) to Al(IV) than FA pastes, further emphasizing its superior reactivity. These findings also confirmed that GGBFS is more reactive than FA in alkaline environments, producing a greater quantity of stable Al-containing phases.

Although the dissolution behavior of MK, GGBFS, and FA is discussed individually throughout this section, a simplified cross-material comparison is provided in Table 5 to summarize qualitative trends reported in the literature for different classes of alkaline activators.

As summarized in Table 5, hydroxide-based activators generally promote higher dissolution tendencies for all three precursors, while silicate-based systems exhibit more moderate dissolution accompanied by the formation of more polymerized binding phases. Clear differences among precursors are

evident, with MK showing high aluminosilicate reactivity, GGBFS favoring Ca-rich C–(A)–S–H formation, and FA exhibiting comparatively slower dissolution that limits early-age reactivity under mild activation conditions. These trends are consistent with the mechanistic discussions presented in Sections 3 and 4. Key topics, along with research gaps and outstanding questions in this area, are summarized in Table 6.

5. Modeling approaches

This section explores computational modeling techniques at the nanoscale level to investigate pozzolanic materials and their impact on dissolution and reactivity. Specifically, it highlights studies employing simulation approaches such as MD, and DFT to examine the underlying mechanisms of dissolution, reaction kinetics, and microstructural evolution in pozzolanic systems.

White et al.[241] combined DFT and pair distribution function (PDF) analysis to uncover the atomic structure of MK. Through an iterative process that refined real-space data from neutron PDF analysis alongside DFT-based geometry optimization, they

Table 5 Qualitative trends in dissolution behavior and dominant reaction products of MK, GGBFS, and FA under representative alkaline activators, as discussed in this review

Material	Activator type	Relative dissolution tendency	Dominant reaction products
MK	Hydroxide-based (e.g., NaOH)	Relatively high	N–A–S–H, aluminosilicate gels
MK	Silicate-based	Moderate	Si-rich N–A–S–H
MK	Ca-based (CH)	Low	C–A–S–H (limited extent)
GGBFS	Hydroxide-based	Relatively high	C–(A)–S–H
GGBFS	Silicate-based	Moderate	C–(A)–S–H
FA	Hydroxide-based	Moderate to low	N–A–S–H
FA	Ca-based (CH)	Low	Limited C–S–H

Table 6 Slag and fly ash-Priority research topic & key question

Topics	Key research questions to be solved
Slag and fly ash structures (GGBFS and FA)	How do differences in composition and structure affect the reactivity and performance of GGBFS and FA in cement and geopolymer systems?
Dissolution and reactivity of GGBFS and FA	How do variations in composition, particle size, activators, and curing conditions affect the reactivity and strength of alkali-activated GGBFS and FA binders?
Impact of alkaline activators on GGBFS and FA reactivity	How do changes in activator type, concentration, and temperature affect dissolution rates, reaction mechanisms, and properties of alkali-activated GGBFS and FA?

developed a structurally accurate and energetically stable model consistent with experimental observations. By eliminating the need for chemical constraints in modeling, this approach enables precise control over MK's structural characteristics, allowing for optimized reactivity and mechanical properties in practical applications. In the model (Fig. 4) presented in,[241] MK is depicted as a layered structure with a Si–O layer and an Al–O(H) layer in a 1 : 1 ratio. All –OH groups are bonded to the Al_2O_3 layer. The model includes Al atoms with 3, 4, and 5 coordination states. The lattice parameters for MK are $a = 30.0354$ Å, $b = 34.6246$ Å, $c = 43.1892$ Å, with the angles $\alpha = 91.926°$, $\beta = 105.046°$, and $\gamma = 89.797°$. Further, White et al.[242] used a multiscale simulation methodology combining DFT and CGMC modeling to investigate the molecular mechanisms governing the dissolution and reactivity of MK in alkaline solutions during geopolymerization. They simulated three systems with varying SiO_2 concentrations in the activating solutions: hydroxide-activated, hydroxide/silicate-activated, and silicate-activated systems. This model described the dissolution of MK, where Al was preferentially released from strained Al_2O_3 layers, leaving behind a silica-enriched residue. The results revealed that the SiO_2 concentration in the activating solution significantly influenced the reactivity and dissolution mechanisms. In hydroxide-activated systems, MK fully dissolved, while in silicate-activated systems, aluminosilicate gels nucleated and precipitated on the surface of partially dissolved MK, inhibiting complete dissolution. Additionally, the presence of $(SiO_4)^{4-}$ facilitated the formation of denser gel networks through larger precipitates, an effect linked to Ostwald ripening, which was observed for the first time in geopolymer systems. These findings provided critical insights into the dissolution dynamics and structural evolution of MK-based systems under alkaline conditions.

Luo et al.[71] employed a MD model in their study, where they added NaOH and water molecules to the MK structure. Using reactive force field (ReaxFF), they simulated the dissolution and reaction of NaOH-activated MK, ultimately establishing the formation of sodium-alumino-silicate-hydrate (N–A–S–H) gel. The results showed that in NaOH solution, the layered structure of MK was disrupted, leading to the formation of SiO_4 and AlO_4 monomers. These monomers then gradually underwent condensation. During the dissolution process, Al dissolved earlier than Si, with Al preferentially participating in the geopolymerization reaction before Si.

The transition of Kln to MK through dehydroxylation involves significant structural changes that influence its

reactivity, as revealed by Sperinck et al.[117] Through MD simulations, it was observed that the removal of structural water causes Al atoms to migrate into nearby vacancies, leading to a buckling effect in the aluminosilicate layers. This migration alters Al's coordination from octahedral to a mix of tetrahedral and five-fold configurations, resulting in localized areas with varied Al densities. These regions exhibit distinct zones of reactivity, with some demonstrating enhanced dissolution potential. The structural disorder introduced during dehydroxylation is identified as a critical factor in defining the reactivity of MK, particularly in its role as a pozzolanic material.

The $(SiO_4)^{4-}$ dissolution of MK in water was investigated using a DFT computational approach, revealing critical differences in activation energy requirements, as shown by Izadifar et al.[31] The activation energy to break the oxo-bridging covalent bond between two silicates was found to be 97% higher than that required to break the ionic bond between $(SiO_4)^{4-}$ and $Al(OH)_4^-$ units. However, for the complete dissociation of $(SiO_4)^{4-}$ tetrahedra, the energy needed to break the ionic bond with the last Al_2O_3 neighbour was 13% higher than that for breaking the covalent bond with the last $(SiO_4)^{4-}$ neighbour. In another research, they employed DFT to explore the dissolution behavior of $(SiO_4)^{4-}$ tetrahedra in MK under alkaline conditions, focusing on bond dissociation and reactivity.[110] The findings indicate that KOH typically exhibits lower activation energy compared to NaOH, especially when van der Waals (vdW) forces are considered. They also reveal that initiating the dissolution of silicate structures demands less energy and underscore the important role played by the cations' surrounding hydration shells. Most recently, Izadifar et al.[243] computed the atomistic activation energy (ΔE_a) at the transition state for dissolution of aluminate species, leading to the formation of aluminum hydroxide hydrate $Al(OH)_3(H_2O)_3$ in an alkaline medium in MK using a machine-learning force field (MLFF)[244–247] derived from DFT, utilizing improved dimer method (IDM) to assess the variation in reaction enthalpy under conditions far-from-equilibrium. The findings revealed that smaller hydration shells around KOH and NaOH resulted in lower ΔE_a for the dissolution of aluminate species by enhancing cation–surface interactions and promoting bond breaking within the aluminosilicate structure. Under the same hydration shell conditions, NaOH exhibited a higher activation energy than KOH, regardless of the presence of vdW interactions. Without vdW interactions, the system faces a greater energy barrier, making the activation process less efficient.

Izadifar et al.[111] applied a 3D off-lattice CGMC method to model the polymerization of alkaline aluminosilicate gels at a system of pH 11, focusing on their nanoparticle sizes and pore size distributions. To inform the simulation, they utilized a reference table of Gibbs free energy values for dimerization reactions involving four distinct monomer types, sourced from DFT-based calculations reported by White et al.[248] In this approach, the polymerization of silicate monomers, modeled as particles within the silicate-activated system, was simulated to reach equilibrium at an energy level of 934 kJ mol^{-1} over the course of 1 000 000 iterations. The results indicated that 91.80% of the silicate particles participated in cluster formation. In another study, Valencia et al.[112] used CGMC simulations supported by DFT-derived parameters to study the dissolution and reactivity of MK in silicate-activated solutions at pH 11, 12, and 13. They found that MK dissolved faster and more completely at pH 11 and 12, releasing $(SiO_4)^{4-}$ and $Al(OH)_4^-$ monomers that actively participated in polycondensation and gel formation. At pH 13, dissolution was slower, leading to a higher proportion of unreacted $(SiO_4)^{4-}$ monomers and a less dense geopolymer structure with larger pores. The results highlighted that very high pH levels reduce MK reactivity and gel formation efficiency. Moreover, Izadifar et al.[113] employed graphene nanosheets to investigate the nucleation process leading to the formation of geopolymer nanocomposites. Their main results showed that the system with the graphene nanosheet had 4.34% fewer particles involved in cluster formation compared to the system without it. However, the graphene-containing system displayed 1.65% more favorable energy. This difference arises because the adsorption energy on the graphene nanosheet (heterogeneous nucleation) is weaker than that in homogeneous particle nucleation.

The dissolution of MK, identified as a key step in forming a cross-linked geopolymer network, was investigated using ReaxFF simulations by Sekkal and Zaoui.[249] The study modeled the polymerization of aluminosilicate oligomers under alkaline conditions, revealing its critical role in geopolymer formation. The addition of carbon nanotubes (CNTs) influenced this process by interacting with the geopolymer matrix and altering its structural properties. At an optimum concentration of 1.08 wt%, pristine CNTs enhanced reactivity and polymerization, improving mechanical properties by facilitating better aluminosilicate gel formation, while higher concentrations led to agglomeration and reduced reactivity. Functionalized CNT-oxide, with covalent bonds formed through C–OH interactions, further increased the density and structural cohesion of the geopolymer, improving diffusion and reactivity.

Chen et al.[250]'s MD study on N–A–S–H gels showed that lower Si/Al ratios created a more compact and crosslinked structure, enhancing stability, while higher ratios yielded a looser network with increased reactivity. The presence of five-fold coordinated Al (Al^V), along with tetrahedral and occasional six-fold coordinated (Al^{VI}), contributed to structural diversity and reactivity. Higher Si/Al ratios increased interlayer spacing, further impacting the gel's reactivity by creating more accessible reactive sites. This work underscored how adjusting the Si/Al ratio could tailor N–A–S–H gel properties for optimized geopolymer performance.

A comparison of the reactivity and dissolution behaviour of MK and GGBFS in NaOH solutions revealed significant differences in their structural responses to alkali activation. MD ReaxFF simulations by Hong et al.[251] showed that MK experienced substantial structural disruption, with sodium ions penetrating its layers and depolymerizing Si chains into monomers. This destabilization extended to Al chains, releasing Al tetrahedral units that acted as precursors for N–A–S–H gel formation, demonstrating MK's high reactivity and solubility under alkaline conditions. In contrast, the GGBFS system exhibited greater structural stability in the same environment. Ca ions were released from the GGBFS interlayers, but the Si and Al frameworks largely retained their layered structure. Ca ions played a crucial role in stabilizing the GGBFS, maintaining its integrity and delaying significant depolymerization. These findings emphasized the higher dissolution and reactivity of MK compared to the more structurally stable GGBFS system, offering valuable insights into the chemical mechanisms driving alkali-activated materials. Guo et al.[252] compared the early stages of geopolymer formation between MK and GGBFS, using MD simulations. They proposed a two-step process involving mineral deconstruction followed by oligomer polymerization. Fig. 11 illustrates that monomers and dimer of $(SiO_4)^{4-}$ tetrahedra, along with other oligomers, form in regions exposed to NaOH and serve as key precursors for the development of calcium–(sodium–)alumina–silicate–hydrate C–(N–)A–S–H gels. The study found that the role of NaOH differs between low-Ca (MK) and high-Ca GGBFS systems. In the low-Ca system, Na$^+$ ions substitute for Ca^{2+}, contributing to the network framework. Conversely, in the high-Ca system, NaOH primarily acts
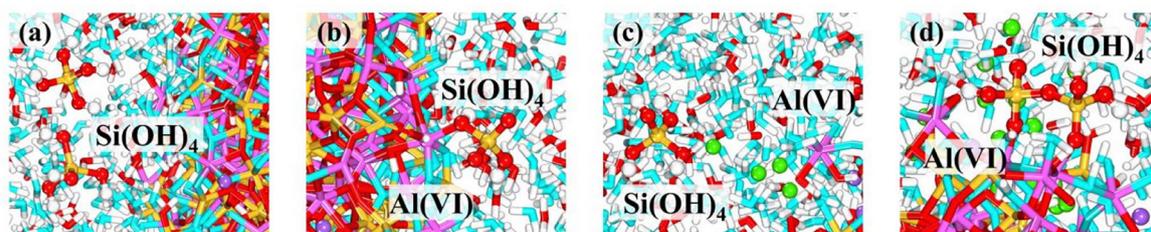
Fig. 11 Comparison of oligomer dissolution in alkali–activated MK and GGBFS: (a) and (b) oligomers dissolved in the MK system following alkali activation (c) and (d) oligomers dissolved in the GGBFS system after alkali activation;[252] reproduced from Guo et al., 2024,[252] licensed under CC BY 4.0.

Table 7 Modeling approach- priority research topic & key question

Topics	Key research questions to be solved
Computational models (DFT, MD, CGMC)	How do nanoscale dissolution and reaction mechanisms govern the reactivity and structural evolution of pozzolanic materials?
Structural reactivity differences (MK vs GGBFS)	Why does MK exhibit higher dissolution and reactivity than GGBFS under alkaline activation, and how do their structural roles differ?
Role of chemical factors (pH, ions, additives)	How do pH levels, ion concentrations, and additives like CNTs or graphene influence geopolymerization kinetics and gel formation?

as an activator, facilitating faster gel formation. The findings also highlighted the stability of Si atoms and the reactivity of Al ions, which undergo structural changes to become part of the geopolymer gel.

The dissolution of NaOH-activated GGBFS was analysed by Gong and White[253] used *in situ* X-ray total scattering, PDF analysis, and MD simulations. Structural models of the amorphous GGBFS were constructed and validated through experimental data, revealing that dissolution disrupted Ca–O and Si–O correlations in the short- and medium-range order. The kinetics of dissolution followed a logarithmic time-dependence, and (C–(N–)A–S–H) gel was identified as the primary reaction product. In another study, Gong and White[254] investigated how variations in Mg/Ca ratios influenced the dissolution rates of amorphous aluminosilicate glasses in alkaline environments. Using force field-based MD simulations, they analyzed structural changes in quaternary $CaO–(MgO)–Al_2O_3–SiO_2$ (CMAS) and ternary $CaO–Al_2O_3–SiO_2$ (CAS) glasses. The study revealed that higher Mg/Ca ratios promoted the formation of highly reactive free oxygen sites, enhancing dissolution rates and providing valuable insights for optimizing GGBFS-like materials in sustainable cement applications.

Huang and Wang[255] examined the effects of varying Mg/Si molar ratios on the structural evolution and reaction mechanisms of AAS gels. Reactive MD simulations using the ReaxFF force field and first-principles DFT calculations were employed to investigate polycondensation reactions among Si-Al monomers. It was determined that Mg/Si ratios significantly influenced GGBFS reactivity, with optimal polycondensation observed at Mg/Si ratios of 0.20 and 0.25. The dissolution and subsequent reactions were driven by the coordination of Mg^{2+} and Ca^{2+} ions with non-bridging oxygens, enhancing polymerization and providing nanoscale insights into Mg's role in optimizing gel structures for sustainable materials.

Oey *et al.*[212] investigated the dissolution kinetics of glassy aluminosilicates, similar to FA, by examining how the atomic structure influences reactivity. MD simulations and topological constraint theory revealed that dissolution rates are governed by the atomic network's rigidity, which depends on bond-stretching and bond-bending constraints. Strong Si–O bonds enhance structural stability, while alkali and alkaline-earth elements disrupt the network by creating non-bridging oxygens (NBOs), accelerating dissolution. They suggested that Al plays a counterbalancing role, stabilizing the network by reducing NBOs and forming stable oxygen clusters. Interestingly, while Ca generally boosts dissolution rates, they found exceptions

that challenge traditional classifications of FA and emphasize the importance of a network-based analysis for accurately predicting reactivity. Key topics, along with research gaps and outstanding questions in this area, are summarized in Table 7.

6. Summary of findings

Kln begins its life as a tightly structured 1 : 1 clay mineral, with one sheet of silicate tetrahedra linked to one sheet of Al octahedra. In its natural form, it is stable and ordered, but when heated between 400 and 850 °C, a transformation begins. Around 300 °C, water molecules are driven off. Between 350 and 700 °C, a more profound change DHX, breaks hydroxyl bonds, distorting the crystal lattice and creating the highly reactive, amorphous form known as metakaolin (MK). Above 800 °C, the structure recrystallizes, losing much of its reactivity. The temperature, heating rate, particle size, morphology, and even the stacking of layers determine exactly when and how this transformation occurs. Disordered kaolinite dehydroxylates at lower temperatures than ordered kaolinite. In kaolinite, Al sits neatly in six-fold coordination (Al^{VI}). As DHX progresses, much of it shifts to five-fold coordination (Al^{V}), a form especially prone to dissolve in alkaline solutions. If heating goes too far, Al settles into a more stable tetrahedral coordination (Al^{IV}), which reacts more slowly. MK with high Al^{V} content, often produced by partial DHX at 600–800 °C, shows the greatest reactivity.

Once transformed, MK meets its most important partner: the alkaline activator. In strong bases like NaOH or KOH, hydroxide ions attack the aluminosilicate network, breaking Si–O–Si and Si-O-Al bonds and releasing silicate (SiO_4^{4-}) and aluminate $Al(OH)_4^-$ ions into solution. NaOH proves more aggressive than KOH, stripping away the network more completely. Dissolution is influenced by pH, alkali concentration, calcination temperature, particle size, and Si/Al ratio. High alkalinity can exfoliate MK layers, increasing surface exposure. The dissolved species quickly polymerize into gels, sometimes zeolitic, sometimes dense aluminosilicate networks, depending on activator type and concentration. An optimal Na/Al molar ratio of ∼1.1 maximizes reaction extent; further increase offers no benefit. CH can steer reactions toward C–S–H gel formation, though at high pH it can hinder network growth. Even potassium silicate solutions can create strong, ceramic-like binders if curing and heat-treatment conditions are well controlled.

Parallel to MK's story runs that of ground granulated blast furnace slag (GGBFS) and fly ash (FA). GGBFS, born from molten iron slag quenched to a glassy state, carries Ca, Si, Al,

and Mg in a loosely polymerized network. Rapid cooling maximizes its amorphous content and reactivity. Its reactivity is influenced by MgO and Al_2O_3 contents, particle size, cooling rate, and the activator used. High MgO promotes hydrotalcite formation; Al_2O_3 boosts early hydration and strength. FA, in contrast, comes from coal combustion, its tiny spheres of glassy aluminosilicate varying widely in Ca content. Class C ashes, richer in Ca, react faster; Class F ashes, leaner in Ca, require stronger activation. FA reactivity depends on glass phase composition, fineness, Ca content, and curing temperature. In alkaline solutions, S ions can synergistically enhance dissolution, modifying the surface gel to promote further leaching of Al and Si. When an activator is added, GGBFS often reacts more readily than FA, especially in NaOH or sodium silicate solutions. NaOH gives rapid early reactions; sodium silicate builds denser long-term structures; sodium carbonate delays setting due to low initial pH. FA responds more slowly, but fineness, higher Ca content, sulfates, and elevated curing temperatures all boost its dissolution and reactivity.

Behind the laboratory work, computational modeling paints a deeper picture. DFT, MD, CGMC simulations reveal atomic-scale mechanisms. MK's layered structure collapses quickly in NaOH, releasing Al before Si. GGBFS holds together longer; Ca leaches first, stabilizing the structure before breakdown. High pH and optimal ion chemistry promote denser gel networks; excess silica in the activator can slow dissolution by forming early surface gels. Hydration shell effects differ between Na^+ and K^+, influencing dissolution energetics. Mg can optimize polycondensation in GGBFS gels, improving strength. Additives like carbon nanotubes or graphene alter nucleation and gel properties, sometimes densifying the network, sometimes slowing particle aggregation.

From this, several findings emerge:

- MK reactivity peaks when calcined near 700 °C with abundant Al^V.

- An optimal Na/Al molar ratio of $\sim$1.1 maximizes dissolution; higher ratios offer no extra benefit.

- NaOH is the most effective activator for MK and FA dissolution; NS builds long-term strength; Na_2CO_3 slows early setting.

- GGBFS benefits from high Ca and Mg contents, forming C–S–H and hydrotalcite; FA benefits most from fineness, Ca, sulfates, and heat.

- Disorder and amorphicity in raw materials lower dissolution energy barriers.

- Modeling confirms different roles of Al and Si in dissolution, the stabilizing effect of Ca in slag, hydration shell effects of Na^+/K^+, and Mg's role in strengthening GGBFS gels.

The combined experimental and modeling evidence offers a clear direction: control the precursor's structure before activation, choose activators carefully, and tailor chemistry for the desired gel. In this way, kaolinite, slag, and fly ash can be transformed from industrial byproducts into the building blocks of durable, sustainable binders.

Although this review emphasizes fundamental dissolution mechanisms, these transformations directly control concrete performance. Rapid dissolution of MK in NaOH-rich systems promotes early gel formation and high early strength, but excessive alkalinity may increase porosity and shrinkage. In contrast, GGBFS dissolution coupled with Ca availability favors continuous C–(A)–S–H formation, improving long-term strength and durability. FA exhibits slower dissolution, requiring elevated temperature or alkali concentration to contribute effectively at early ages. From a practical perspective, MK-rich systems benefit from moderate alkali concentrations and controlled curing to avoid rapid setting, while GGBFS-based binders are well suited for ambient curing with silicate activators. FA-based systems require either thermal curing or blended activation strategies to achieve sufficient early performance.

7. Conclusion

The main findings, detailed in section 6, highlight the structure evolution and dissolution mechanisms of MK, GGBFS, and FA affected by various activators and curing conditions. The effective valorization of kaolinite, GGBFS, and FA into high-performance, sustainable binders critically depends on understanding their structural transformations and activation mechanisms. This review demonstrates that optimizing precursor modification, calcination parameters, and activator selection is crucial for enhancing reaction kinetics, tailoring gel microstructures, and improving durability. Integrating advanced experimental characterization with atomic-scale computational methods, including DFT, MD, and CGMC simulations enables a multi-scale perspective on reaction pathways and long-term structural evolution.

Key conclusions

Metakaolin formation: calcination near 700 °C yields highly reactive metakaolin enriched in five-fold coordinated aluminum (Al^V), significantly accelerating dissolution and subsequent gel polymerization. Slight variations in calcination temperature can shift the balance between reactivity and crystallinity. Changes in unit cell volume has been observed during the transformation of Kln to MK and disordered Kln to metadiskaolin.

Activator performance: sodium hydroxide (NaOH) maximizes dissolution efficiency for MK and FA, enabling rapid early-stage reaction rates. Sodium silicate, while slightly slower in initial dissolution, fosters denser and more cross-linked gel networks. Sodium carbonate offers a milder activation route but delays setting, which may benefit applications requiring extended workability.

Structural disorder: increased amorphicity and lattice disorder in precursors reduce dissolution energy barriers, thereby enhancing activation kinetics and broadening processing windows.

Slag (GGBFS) and fly ash (FA) reactivity: GGBFS benefits from its intrinsic Ca and Mg content, promoting the formation of calcium silicate hydrate (C–S–H) and hydrotalcite phases.

FA reactivity is strongly influenced by particle fineness, Ca and sulfate content, and elevated curing temperatures, which accelerate both dissolution and gel growth.

Computational insights: DFT analyses clarify the bond-breaking mechanisms and coordination changes during dissolution; MD simulations reveal dynamic hydration shell behavior and ion–ion interactions; CGMC simulations predict long-term gel polymerization pathways and microstructural evolution.

Collectively, these findings reinforce the necessity of precise precursor engineering, tailored activator chemistry, and integrated experimental–computational workflows for the rational design of durable, sustainable aluminosilicate binders from industrial byproducts. The synergy between empirical data and simulation-driven insights paves the way for predictive material design, reducing trial-and-error approaches and accelerating the transition toward greener construction materials.

It should be emphasized that this review deliberately focuses on single-component pozzolanic systems (MK, GGBFS, and FA) to isolate intrinsic dissolution and reactivity mechanisms. The complexities of multi-binder and blended cement systems were intentionally excluded to avoid convolution of chemical interactions. The mechanistic insights presented here are intended as a foundational framework upon which future studies of multi-component systems can be systematically built.

Conflicts of interest

There are no conflicts to declare.

Abbreviations

SCM	Supplementary cementitious material
PC	Portland cement
OPC	Ordinary Portland cement
DHX	Dehydroxylation
Si	Silicon
Al	Aluminum
Ca	Calcium
S	Sulfate
Mg	Magnesium
C–S–H	Calcium–silicate–hydrates
C–A–S–H	Calcium–alumino–silicate–hydrates
C–A–H	Calcium-aluminate-hydrate
XRD	X-ray diffraction
DSC	Differential scanning calorimetry
$(SiO_4)^{4-}$	Silicate
$Al(OH)_4^-$	Aluminate
MD	Molecular dynamics
DFT	Density functional theory
IDM	Improved dimer method
ReaxFF	Reactive force field
ΔE_a	Activation energy
vdW	van der Waals
MLFF	Machine-learning force field
PDF	Pair distribution function
SEM	Scanning electron microscopics (SEMs)
ITC	Isothermal titration calorimetry
TGA	Thermogravimetric analysis
EDS	Energy dispersive X-ray spectroscopy
NMR	Nuclear magnetic resonance
AAS	Alkali-activated slag
HT	Hydrotalcite
NBO	Non-bridging oxygen
N–A–S–H	Sodium–alumino–silicate–hydrate
(C–(N–)A–S–H)	Calcium–(sodium–)alumino–silicate–hydrate
CGMC	Coarse-grained Monte Carlo
CNT	Carbon nanotube
CMAS	$CaO-(MgO)-Al_2O_3-SiO_2$

Data availability

All relevant data supporting this study are fully included in the Results and Discussion section of this article.

Acknowledgements

References

1 O. R. Kavitha, V. M. Shanthi, G. P. Arulraj and V. R. Sivakumar, Microstructural Studies on Eco-Friendly and Durable Self-Compacting Concrete Blended with Metakaolin, *Appl. Clay Sci.*, 2016, **124–125**, 143–149, DOI: 10.1016/j.clay.2016.02.011.

2 A. Perrot, Y. Jacquet, J. F. Caron, R. Mesnil, N. Ducoulombier, V. De Bono, J. Sanjayan, S. Ramakrishnan, H. Kloft, J. Gosslar, S. Muthukrishnan, V. Mechtcherine, T. Wangler, J. L. Provis, K. Dörfler, E. Krakovska, N. Roussel and E. Keita, Snapshot on 3D Printing with Alternative Binders and Materials: Earth, Geopolymers, Gypsum and Low Carbon Concrete, *Cem. Concr. Res.*, 2024, **185**, 107651, DOI: 10.1016/j.cemconres.2024.107651.

3 P. D. Nukah, S. J. Abbey, C. A. Booth and J. Oti, Development of Low Carbon Concrete and Prospective of Geopolymer Concrete Using Lightweight Coarse Aggregate and Cement Replacement Materials, *Constr. Build. Mater.*, 2024, **428**, 136295, DOI: 10.1016/j.conbuildmat.2024.136295.

4 E. Gartner and H. Hirao, A Review of Alternative Approaches to the Reduction of CO_2 Emissions Associated with the Manufacture of the Binder Phase in Concrete,

Cem. Concr. Res., 2015, **78**, 126–142, DOI: 10.1016/j.cemconres.2015.04.012.

5 Y. Zhao, J. Qiu, S. Zhang, Z. Guo, P. Wu, X. Sun and X. Gu, Low Carbon Binder Modified by Calcined Quarry Dust for Cemented Paste Backfill and the Associated Environmental Assessments, *J. Environ. Manage.*, 2021, **300**, 113760, DOI: 10.1016/j.jenvman.2021.113760.

6 R. Fernandez, F. Martirena and K. L. Scrivener, The Origin of the Pozzolanic Activity of Calcined Clay Minerals: A Comparison between Kaolinite, Illite and Montmorillonite, *Cem. Concr. Res.*, 2011, **41**(1), 113–122, DOI: 10.1016/j.cemconres.2010.09.013.

7 A. Tironi, M. A. Trezza, A. N. Scian and E. F. Irassar, Assessment of Pozzolanic Activity of Different Calcined Clays, *Cem. Concr. Compos.*, 2013, **37**, 319–327, DOI: 10.1016/j.cemconcomp.2013.01.002.

8 V. G. Papadakis, S. Antiohos and S. Tsimas, Supplementary Cementing Materials in Concrete: Part II: A Fundamental Estimation of the Efficiency Factor, *Cem. Concr. Res.*, 2002, **32**(10), 1533–1538, DOI: 10.1016/S0008-8846(02)00829-3.

9 R. Snellings, G. Mertens and J. Elsen, Supplementary Cementitious Materials, *Rev. Mineral. Geochem.*, 2012, **74**(1), 211–278, DOI: 10.2138/rmg.2012.74.6.

10 G. Li, C. Zhou, W. Ahmad, K. I. Usanova, M. Karelina, A. M. Mohamed and R. Khallaf, Fly Ash Application as Supplementary Cementitious Material: A Review, *Materials*, 2022, **15**(7), 2664, DOI: 10.3390/ma15072664.

11 J. L. Provis, Alkali-Activated Materials, *Cem. Concr. Res.*, 2018, **114**, 40–48, DOI: 10.1016/j.cemconres.2017.02.009.

12 B. Singh, G. Ishwarya, M. Gupta and S. K. Bhattacharyya, Geopolymer Concrete: A Review of Some Recent Developments, *Constr. Build. Mater.*, 2015, **85**, 78–90, DOI: 10.1016/j.conbuildmat.2015.03.036.

13 C.-K. Ma, A. Z. Awang and W. Omar, Structural and Material Performance of Geopolymer Concrete: A Review, *Constr. Build. Mater.*, 2018, **186**, 90–102, DOI: 10.1016/j.conbuildmat.2018.07.111.

14 W. K. Part, M. Ramli and C. B. Cheah, An Overview on the Influence of Various Factors on the Properties of Geopolymer Concrete Derived from Industrial By-Products, *Constr. Build. Mater.*, 2015, **77**, 370–395, DOI: 10.1016/j.conbuildmat.2014.12.065.

15 F. Farooq, X. Jin, M. Faisal Javed, A. Akbar, M. Izhar Shah, F. Aslam and R. Alyousef, Geopolymer Concrete as Sustainable Material: A State of the Art Review, *Constr. Build. Mater.*, 2021, **306**, 124762, DOI: 10.1016/j.conbuildmat.2021.124762.

16 K. H. Mo, U. J. Alengaram and M. Z. Jumaat, Structural Performance of Reinforced Geopolymer Concrete Members: A Review, *Constr. Build. Mater.*, 2016, **120**, 251–264, DOI: 10.1016/j.conbuildmat.2016.05.088.

17 L. Dubyey, N. Ukrainczyk, S. Yadav, M. Izadifar, J. J. Schneider and E. Koenders, Carbon Nanotubes and Nanohorns in Geopolymers: A Study on Chemical, Physical and Mechanical Properties, *Mater. Des.*, 2024, **240**, 112851, DOI: 10.1016/j.matdes.2024.112851.

18 W. Sekkal, M. Izadifar, A. Zaoui, N. Ukrainczyk and E. Koenders, Theoretical Investigation of Protective Graphene-Coated Metakaolin Geopolymer Interface under Moisture and Chemical Composition Effects, *Powder Technol.*, 2023, **430**, 119007, DOI: 10.1016/j.powtec.2023.119007.

19 A. R. Lori, R. M. Novais, G. Ascensão, F. Fernandes, N. Ranjbar and J. Spangenberg, Chemically Foamed Geopolymers for 3D Printing Applications, *Cem. Concr. Compos.*, 2025, **161**, 106116, DOI: 10.1016/j.cemconcomp.2025.106116.

20 S. Rahemipoor, M. Hasany, M. Mehrali, K. Almdal, N. Ranjbar and M. Mehrali, Phase Change Materials Incorporation into 3D Printed Geopolymer Cement: A Sustainable Approach to Enhance the Comfort and Energy Efficiency of Buildings, *J. Cleaner Prod.*, 2023, **417**, 138005, DOI: 10.1016/j.jclepro.2023.138005.

21 S. Hollanders, R. Adriaens, J. Skibsted, Ö. Cizer and J. Elsen, Pozzolanic Reactivity of Pure Calcined Clays, *Appl. Clay Sci.*, 2016, **132–133**, 552–560, DOI: 10.1016/j.clay.2016.08.003.

22 N. Beuntner and K.-C. Thienel, Pozzolanic Efficiency of Calcined Clays in Blended Cements with a Focus on Early Hydration, *Adv. Cem. Res.*, 2022, **34**(8), 341–355, DOI: 10.1680/jadcr.21.00034.

23 J. L. Provis, Geopolymers and Other Alkali Activated Materials: Why, How, and What?, *Mater. Struct.*, 2014, **47**(1), 11–25, DOI: 10.1617/s11527-013-0211-5.

24 B. B. Jindal, T. Alomayri, A. Hasan and C. R. Kaze, Geopolymer Concrete with Metakaolin for Sustainability: A Comprehensive Review on Raw Material's Properties, Synthesis, Performance, and Potential Application, *Environ. Sci. Pollut. Res.*, 2023, **30**(10), 25299–25324, DOI: 10.1007/s11356-021-17849-w.

25 C. Ferone, F. Colangelo, G. Roviello, D. Asprone, C. Menna, A. Balsamo, A. Prota, R. Cioffi and G. Manfredi, Application-Oriented Chemical Optimization of a Metakaolin Based Geopolymer, *Materials*, 2013, **6**(5), 1920–1939, DOI: 10.3390/ma6051920.

26 A. M. Rashad, Metakaolin as Cementitious Material: History, Scours, Production and Composition – A Comprehensive Overview, *Constr. Build. Mater.*, 2013, **41**, 303–318, DOI: 10.1016/j.conbuildmat.2012.12.001.

27 E.-H. Kadri, S. Kenai, K. Ezziane, R. Siddique and G. De Schutter, Influence of Metakaolin and Silica Fume on the Heat of Hydration and Compressive Strength Development of Mortar, *Appl. Clay Sci.*, 2011, **53**(4), 704–708, DOI: 10.1016/j.clay.2011.06.008.

28 A. M. Ramezanianpour and R. D. Hooton, A Study on Hydration, Compressive Strength, and Porosity of Portland-Limestone Cement Mixes Containing SCMs, *Cem. Concr. Compos.*, 2014, **51**, 1–13, DOI: 10.1016/j.cemconcomp.2014.03.006.

29 D. Khale and R. Chaudhary, Mechanism of Geopolymerization and Factors Influencing Its Development: A Review, *J. Mater. Sci.*, 2007, **42**(3), 729–746, DOI: 10.1007/s10853-006-0401-4.

30 Z. Zhang, H. Wang, J. L. Provis, F. Bullen, A. Reid and Y. Zhu, Quantitative Kinetic and Structural Analysis of

Geopolymers. Part 1. The Activation of Metakaolin with Sodium Hydroxide, *Thermochim. Acta*, 2012, **539**, 23–33, DOI: 10.1016/j.tca.2012.03.021.

31 M. Izadifar, N. Ukrainczyk and E. Koenders, Silicate Dissolution Mechanism from Metakaolinite Using Density Functional Theory, *Nanomaterials*, 2023, **13**(7), 1196.

32 H. Y. Zhang, V. Kodur, S. L. Qi, L. Cao and B. Wu, Development of Metakaolin–Fly Ash Based Geopolymers for Fire Resistance Applications, *Constr. Build. Mater.*, 2014, **55**, 38–45, DOI: 10.1016/j.conbuildmat.2014.01.040.

33 S. Scherb, M. Köberl, N. Beuntner, C. Thienel and J. Neubauer, Reactivity of Metakaolin in Alkaline Environment: Correlation of Results from Dissolution Experiments with XRD Quantifications, *Materials*, 2020, **13**, 2214, DOI: 10.3390/ma13102214.

34 C. Shi and R. L. Day, Comparison of Different Methods for Enhancing Reactivity of Pozzolans, *Cem. Concr. Res.*, 2001, **31**(5), 813–818, DOI: 10.1016/S0008-8846(01)00481-1.

35 K. Weise, N. Ukrainczyk and E. Koenders, Pozzolanic Reactions of Metakaolin with Calcium Hydroxide: Review on Hydrate Phase Formations and Effect of Alkali Hydroxides, Carbonates and Sulfates, *Mater. Des.*, 2023, **231**, 112062, DOI: 10.1016/j.matdes.2023.112062.

36 S. Mohammed, Processing, Effect and Reactivity Assessment of Artificial Pozzolans Obtained from Clays and Clay Wastes: A Review, *Constr. Build. Mater.*, 2017, **140**, 10–19, DOI: 10.1016/j.conbuildmat.2017.02.078.

37 M. Kasaniya, A. Alaibani, M. D. A. Thomas and K. A. Riding, Exploring the Efficacy of Emerging Reactivity Tests in Screening Pozzolanic Materials, *Constr. Build. Mater.*, 2022, **325**, 126781, DOI: 10.1016/j.conbuildmat.2022.126781.

38 M. Bauchy, M. J. A. Qomi, F.-J. Ulm and R. J.-M. Pellenq, Order and Disorder in Calcium–Silicate–Hydrate, *J. Chem. Phys.*, 2014, **140**(21), 214503, DOI: 10.1063/1.4878656.

39 M. Izadifar, F. Königer, A. Gerdes, C. Wöll and P. Thissen, Correlation between Composition and Mechanical Properties of Calcium Silicate Hydrates Identified by Infrared Spectroscopy and Density Functional Theory, *J. Phys. Chem. C*, 2019, **123**(17), 10868–10873, DOI: 10.1021/acs.jpcc.8b11920.

40 I. G. Richardson, The Calcium Silicate Hydrates, *Cem. Concr. Res.*, 2008, **38**(2), 137–158, DOI: 10.1016/j.cemconres.2007.11.005.

41 E. John, T. Matschei and D. Stephan, Nucleation Seeding with Calcium Silicate Hydrate – A Review, *Cem. Concr. Res.*, 2018, **113**, 74–85, DOI: 10.1016/j.cemconres.2018.07.003.

42 M. Izadifar, J. S. Dolado, P. Thissen and A. Ayuela, Interactions between Reduced Graphene Oxide with Monomers of (Calcium) Silicate Hydrates: A First-Principles Study, *Nanomaterials*, 2021, **11**(9), 2248, DOI: 10.3390/nano11092248.

43 M. Izadifar, C. Natzeck, K. Emmerich, P. G. Weidler, S. Gohari, C. Burvill and P. Thissen, Unexpected Chemical Activity of a Mineral Surface: The Role of Crystal Water in Tobermorite, *J. Phys. Chem. C*, 2022, **126**(30), 12405–12412, DOI: 10.1021/acs.jpcc.1c10151.

44 M. Izadifar, J. S. Dolado, P. Thissen, N. Ukrainczyk, E. Koenders and A. Ayuela, Theoretical Elastic Constants of Tobermorite Enhanced with Reduced Graphene Oxide through Hydroxyl vs Epoxy Functionalization: A First-Principles Study, *J. Phys. Chem. C*, 2023, **127**(36), 18117–18126, DOI: 10.1021/acs.jpcc.3c03893.

45 C. Li, H. Sun and L. Li, A Review: The Comparison between Alkali-Activated Slag (Si + Ca) and Metakaolin (Si + Al) Cements, *Cem. Concr. Res.*, 2010, **40**(9), 1341–1349, DOI: 10.1016/j.cemconres.2010.03.020.

46 M. Palou, E. Kuzielová, M. Žemlička, R. Novotný and J. Másilko, The Effect of Metakaolin upon the Formation of Ettringite in Metakaolin–Lime–Gypsum Ternary Systems, *J. Therm. Anal. Calorim.*, 2018, **133**(1), 77–86, DOI: 10.1007/s10973-017-6885-0.

47 M. Izadifar, W. Sekkal, L. Dubyey, N. Ukrainczyk, A. Zaoui and E. Koenders, Theoretical Studies of Adsorption Reactions of Aluminosilicate Aqueous Species on Graphene-Based Nanomaterials: Implications for Geopolymer Binders, *ACS Appl. Nano Mater.*, 2023, 3c02438, DOI: 10.1021/acsanm.3c02438.

48 G. C. Isaia, A. L. G. Gastaldini and R. Moraes, Physical and Pozzolanic Action of Mineral Additions on the Mechanical Strength of High-Performance Concrete, *Cem. Concr. Compos.*, 2003, **25**(1), 69–76, DOI: 10.1016/S0958-9465(01)00057-9.

49 A. Goldman and A. Bentur, The Influence of Microfillers on Enhancement of Concrete Strength, *Cem. Concr. Res.*, 1993, **23**(4), 962–972, DOI: 10.1016/0008-8846(93)90050-J.

50 M. Madhkhan and R. Katirai, Effect of Pozzolanic Materials on Mechanical Properties and Aging of Glass Fiber Reinforced Concrete, *Constr. Build. Mater.*, 2019, **225**, 146–158, DOI: 10.1016/j.conbuildmat.2019.07.128.

51 R. Homayoonmehr, A. A. Ramezanianpour and M. Mirdarsoltany, Influence of Metakaolin on Fresh Properties, Mechanical Properties and Corrosion Resistance of Concrete and Its Sustainability Issues: A Review, *J. Build. Eng.*, 2021, **44**, 103011, DOI: 10.1016/j.jobe.2021.103011.

52 A. Fernández-Jiménez, J. G. Palomo and F. Puertas, Alkali-Activated Slag Mortars: Mechanical Strength Behaviour, *Cem. Concr. Res.*, 1999, **29**(8), 1313–1321, DOI: 10.1016/S0008-8846(99)00154-4.

53 F. Massazza, 10 - Pozzolana and Pozzolanic Cements, in *Lea's Chemistry of Cement and Concrete*, Ed. Hewlett, P. C., Butterworth-Heinemann, Oxford, Fourthedn, 1998, pp. 471–635. , DOI: 10.1016/B978-075066256-7/50022-9.

54 J. Péra, S. Husson and B. Guilhot, Influence of Finely Ground Limestone on Cement Hydration, *Cem. Concr. Compos.*, 1999, **21**(2), 99–105, DOI: 10.1016/S0958-9465(98)00020-1.

55 D. D. Bui, J. Hu and P. Stroeven, Particle Size Effect on the Strength of Rice Husk Ash Blended Gap-Graded Portland Cement Concrete, *Cem. Concr. Compos.*, 2005, **27**(3), 357–366, DOI: 10.1016/j.cemconcomp.2004.05.002.

56 F. Puertas, S. Martínez-Ramírez, S. Alonso and T. Vázquez, Alkali-Activated Fly Ash/Slag Cements: Strength Behaviour

and Hydration Products, *Cem. Concr. Res.*, 2000, **30**(10), 1625–1632, DOI: 10.1016/S0008-8846(00)00298-2.

57 M. Atkins, F. P. Glasser and J. J. Jack, Zeolite P in Cements: Its Potential for Immobilizing Toxic and Radioactive Waste Species, *Waste Manage.*, 1995, **15**(2), 127–135, DOI: 10.1016/0956-053X(95)00015-R.

58 J. J. Brooks, Prediction of Setting Time of Fly Ash Concrete, *Mater. J.*, 2002, **99**(6), 591–597.

59 J. C. Swanepoel and C. A. Strydom, Utilisation of Fly Ash in a Geopolymeric Material, *Appl. Geochem.*, 2002, **17**(8), 1143–1148, DOI: 10.1016/S0883-2927(02)00005-7.

60 A. Palomo, M. W. Grutzeck and M. T. Blanco, Alkali-Activated Fly Ashes: A Cement for the Future, *Cem. Concr. Res.*, 1999, **29**(8), 1323–1329, DOI: 10.1016/S0008-8846(98)00243-9.

61 A. V. Kirschner and H. Harmuth, Investigation of Geopolymer Binders with Respect to Their Application for Building Materials, *Ceram.-Silik.*, 2004, **48**(3), 117–120.

62 S. Martinez-Ramirez and A. Palomo, Microstructure Studies on Portland Cement Pastes Obtained in Highly Alkaline Environments, *Cem. Concr. Res.*, 2001, **31**(11), 1581–1585, DOI: 10.1016/S0008-8846(01)00603-2.

63 J. G. S. van Jaarsveld, J. S. J. van Deventer and G. C. Lukey, The Effect of Composition and Temperature on the Properties of Fly Ash- and Kaolinite-Based Geopolymers, *Chem. Eng. J.*, 2002, **89**(1), 63–73, DOI: 10.1016/S1385-8947(02)00025-6.

64 D. Hardjito, S. E. Wallah, D. M. J. Sumajouw and B. V. Rangan, On the Development of Fly Ash-Based Geopolymer Concrete, *Am. Concr. Inst.*, 2004, 467–472.

65 K. Wang, S. P. Shah and A. Mishulovich, Effects of Curing Temperature and NaOH Addition on Hydration and Strength Development of Clinker-Free CKD-Fly Ash Binders, *Cem. Concr. Res.*, 2004, **34**(2), 299–309, DOI: 10.1016/j.cemconres.2003.08.003.

66 J. W. Phair and J. S. J. Van Deventer, Effect of Silicate Activator pH on the Leaching and Material Characteristics of Waste-Based Inorganic Polymers, *Miner. Eng.*, 2001, **14**(3), 289–304, DOI: 10.1016/S0892-6875(01)00002-4.

67 P. Duxson, G. C. Lukey, F. Separovic and J. S. J. van Deventer, Effect of Alkali Cations on Aluminum Incorporation in Geopolymeric Gels, *Ind. Eng. Chem. Res.*, 2005, **44**(4), 832–839, DOI: 10.1021/ie0494216.

68 J. Davidovits, *Geopolymers*, 2005, DOI: 10.1007/bf01912193.

69 S. Chitsaz and A. Tarighat, Molecular Dynamics Simulation of N-A-S-H Geopolymer Macro Molecule Model for Prediction of Its Modulus of Elasticity, *Constr. Build. Mater.*, 2020, **243**, 118176, DOI: 10.1016/j.conbuildmat.2020.118176.

70 P. Duxson, A. Fernández-Jiménez, J. L. Provis, G. C. Lukey, A. Palomo and J. S. J. van Deventer, Geopolymer Technology: The Current State of the Art, *J. Mater. Sci.*, 2007, **42**(9), 2917–2933, DOI: 10.1007/s10853-006-0637-z.

71 X. Luo, X. Tian, J. Wu, X. Yang, Z. Liu, Z. Jiao and H. Peng, Molecular Simulations of the Initial Stage's Induction and Formation Process of N-A-S-H Gel Based on

NaOH-Activated Metakaolin, *J. Non-Cryst. Solids*, 2024, **626**, 122804, DOI: 10.1016/j.jnoncrysol.2023.122804.

72 X. Yao, Z. Zhang, H. Zhu and Y. Chen, Geopolymerization Process of Alkali–Metakaolinite Characterized by Isothermal Calorimetry, *Thermochim. Acta*, 2009, **493**(1), 49–54, DOI: 10.1016/j.tca.2009.04.002.

73 H. Xu and J. S. J. Van Deventer, The Geopolymerisation of Alumino-Silicate Minerals, *Int. J. Miner. Process.*, 2000, **59**(3), 247–266, DOI: 10.1016/S0301-7516(99)00074-5.

74 L. Verdolotti, S. Iannace, M. Lavorgna and R. Lamanna, Geopolymerization Reaction to Consolidate Incoherent Pozzolanic Soil, *J. Mater. Sci.*, 2008, **43**(3), 865–873, DOI: 10.1007/s10853-007-2201-x.

75 G. Görhan, R. Aslaner and O. Şinik, The Effect of Curing on the Properties of Metakaolin and Fly Ash-Based Geopolymer Paste, *Composites, Part B*, 2016, **97**, 329–335, DOI: 10.1016/j.compositesb.2016.05.019.

76 J. Davidovits Properties of geopolymer cements. https://scholar.google.com/scholar_lookup?title=Properties%20of%20geopolymer%20cements&publication_year=1994&author=J.%20Davidovits (accessed 2024-10-08).

77 D. M. J. Sumajouw, D. Hardjito, S. E. Wallah and B. V. Rangan, Fly Ash-Based Geopolymer Concrete: Study of Slender Reinforced Columns, *J. Mater. Sci.*, 2007, **42**(9), 3124–3130, DOI: 10.1007/s10853-006-0523-8.

78 B. B. Sabir, S. Wild and J. Bai, Metakaolin and Calcined Clays as Pozzolans for Concrete: A Review, *Cem. Concr. Compos.*, 2001, **23**(6), 441–454, DOI: 10.1016/S0958-9465(00)00092-5.

79 C. Jian-Xiong, C. Han-bin, X. Pei and Z. Lan-Fang, A Study on Complex Alkali-Slag Environmental Concrete, *Int. Workshop Sustainable Dev. Concr. Technol.*, 2004, 299–307.

80 P. Krivenko, O. Petropavlovsky and H. Vozniuk, Development of Mixture Design of Heat Resistant Alkali-Activated Aluminosilicate Binder-Based Adhesives, *Constr. Build. Mater.*, 2017, **149**, 248–256, DOI: 10.1016/j.conbuildmat.2017.05.138.

81 J. Cabrera and M. F. Rojas, Mechanism of Hydration of the Metakaolin–Lime–Water System, *Cem. Concr. Res.*, 2001, **31**(2), 177–182, DOI: 10.1016/S0008-8846(00)00456-7.

82 P. S. de Silva and F. P. Glasser, Hydration of Cements Based on Metakaolin: Thermochemistry, *Adv. Cem. Res.*, 1990, **3**(12), 167–177, DOI: 10.1680/adcr.1990.3.12.167.

83 M. Frías and J. Cabrera, Influence of MK on the Reaction Kinetics in MK/Lime and MK-Blended Cement Systems at 20 °C, *Cem. Concr. Res.*, 2001, **31**(4), 519–527, DOI: 10.1016/S0008-8846(00)00465-8.

84 G. Deng, Y. He, L. Lu and S. Hu, The Effect of Activators on the Dissolution Characteristics and Occurrence State of Aluminum of Alkali-Activated Metakaolin, *Constr. Build. Mater.*, 2020, **235**, 117451, DOI: 10.1016/j.conbuildmat.2019.117451.

85 K. M. Salah Uddin, M. Izadifar, N. Ukrainczyk, E. Koenders and B. Middendorf, Dissolution of Portlandite in Pure Water: Part 1 Molecular Dynamics (MD) Approach, *Materials*, 2022, **15**(4), 1404, DOI: 10.3390/ma15041404.

86 K. M. Salah Uddin, M. Izadifar, N. Ukrainczyk, E. Koenders and B. Middendorf, Dissolution of β-C2S Cement Clinker:

Part 1 Molecular Dynamics (MD) Approach for Different Crystal Facets, *Materials*, 2022, **15**(18), 6388, DOI: 10.3390/ma15186388.

87 M. Izadifar, N. Ukrainczyk, K. M. Salah Uddin, B. Middendorf and E. Koenders, Dissolution of β-C2S Cement Clinker: Part 2 Atomistic Kinetic Monte Carlo (KMC) Upscaling Approach, *Materials*, 2022, **15**(19), 6716, DOI: 10.3390/ma15196716.

88 M. Izadifar, N. Ukrainczyk, K. M. Salah Uddin, B. Middendorf and E. Koenders, Dissolution of Portlandite in Pure Water: Part 2 Atomistic Kinetic Monte Carlo (KMC) Approach, *Materials*, 2022, **15**(4), 1442, DOI: 10.3390/ma15041442.

89 R. J.-M. Pellenq, A. Kushima, R. Shahsavari, K. J. Van Vliet, M. J. Buehler, S. Yip and F.-J. Ulm, A Realistic Molecular Model of Cement Hydrates, *Proc. Natl. Acad. Sci. U. S. A.*, 2009, **106**(38), 16102–16107, DOI: 10.1073/pnas.0902180106.

90 F. Hong, M. Wang, B. Dong, X. Diao, X. Zhang, K. Pang, Y. Zhang and D. Hou, Molecular Insight into the Pozzolanic Reaction of Metakaolin and Calcium Hydroxide, *Langmuir*, 2023, **39**(10), 3601–3609, DOI: 10.1021/acs.langmuir.2c03115.

91 A. A. Bahraq, M. A. Al-Osta, O. S. Baghabra Al-Amoudi, I. B. Obot, M. Maslehuddin, H.-R. Ahmed and T. A. Saleh, Molecular Simulation of Cement-Based Materials and Their Properties, *Engineering*, 2022, **15**, 165–178, DOI: 10.1016/j.eng.2021.06.023.

92 Y. Zhang, S. Zhang, X. Jiang, Q. Chen, Z. Jiang, J. W. Ju and M. Bauchy, Insights into the Thermal Effect on the Fracture Toughness of Calcium Silicate Hydrate Grains: A Reactive Molecular Dynamics Study, *Cem. Concr. Compos.*, 2022, **134**, 104824, DOI: 10.1016/j.cemconcomp.2022.104824.

93 R. Horstmann, L. Hecht, S. Kloth and M. Vogel, Structural and Dynamical Properties of Liquids in Confinements: A Review of Molecular Dynamics Simulation Studies, *Langmuir*, 2022, **38**(21), 6506–6522, DOI: 10.1021/acs.langmuir.2c00521.

94 S. Al-Hajri, D. Bahamon, M. M. Rahman, M. Haroun and L. F. Vega, Adhesion and Cohesion of Silica Surfaces with Quartz Cement: A Molecular Simulations Study, *ACS Omega*, 2022, **7**(26), 22303–22316, DOI: 10.1021/acsomega.2c01129.

95 D. Hou, J. Xu, Y. Zhang and G. Sun, Insights into the Molecular Structure and Reinforcement Mechanism of the Hydrogel-Cement Nanocomposite: An Experimental and Molecular Dynamics Study, *Composites, Part B*, 2019, **177**, 107421, DOI: 10.1016/j.compositesb.2019.107421.

96 C. Jiang, K. Li, J. Zhang, Q. Qin, Z. Liu, W. Liang, M. Sun and Z. Wang, The Effect of CaO(MgO) on the Structure and Properties of Aluminosilicate System by Molecular Dynamics Simulation, *J. Mol. Liq.*, 2018, **268**, 762–769, DOI: 10.1016/j.molliq.2018.07.123.

97 B. Mortazavi and S. Ahzi, Thermal Conductivity and Tensile Response of Defective Graphene: A Molecular Dynamics Study, *Carbon*, 2013, **63**, 460–470, DOI: 10.1016/j.carbon.2013.07.017.

98 M. Izadifar, P. Thissen, R. Abadi, A. N. Jam, S. Gohari, C. Burvill and T. Rabczuk, Fracture Toughness of Various Percentage of Doping of Boron Atoms on the Mechanical Properties of Polycrystalline Graphene: A Molecular Dynamics Study, *Phys. E*, 2019, **114**, 113614, DOI: 10.1016/j.physe.2019.113614.

99 A. N. Jam, R. Abadi, M. Izadifar and T. Rabczuk, Molecular Dynamics Study on the Mechanical Properties of Carbon Doped Single-Layer Polycrystalline Boron-Nitride Nanosheets, *Comput. Mater. Sci.*, 2018, **153**, 16–27, DOI: 10.1016/j.commatsci.2018.06.011.

100 A. N. Jam, N. N. Jam, M. Izadifar and T. Rabczuk, Molecular Dynamics Study on the Crack Propagation in Carbon Doped Polycrystalline Boron-Nitride Nanosheets, *Comput. Mater. Sci.*, 2022, **203**, 111066, DOI: 10.1016/j.commatsci.2021.111066.

101 B. Mortazavi, G. Cuniberti and T. Rabczuk, Mechanical Properties and Thermal Conductivity of Graphitic Carbon Nitride: A Molecular Dynamics Study, *Comput. Mater. Sci.*, 2015, **99**, 285–289, DOI: 10.1016/j.commatsci.2014.12.036.

102 A. H. N. Shirazi, R. Abadi, M. Izadifar, N. Alajlan and T. Rabczuk, Mechanical Responses of Pristine and Defective C3N Nanosheets Studied by Molecular Dynamics Simulations, *Comput. Mater. Sci.*, 2018, **147**, 316–321, DOI: 10.1016/j.commatsci.2018.01.058.

103 Q. Zhang, B. Mortazavi, X. Zhuang and F. Aldakheel, Exploring the Mechanical Properties of Two-Dimensional Carbon-Nitride Polymer Nanocomposites by Molecular Dynamics Simulations, *Compos. Struct.*, 2022, **281**, 115004, DOI: 10.1016/j.compstruct.2021.115004.

104 M. Izadifar, R. Abadi, A. H. Nezhad Shirazi, N. Alajlan and T. Rabczuk, Nanopores Creation in Boron and Nitrogen Doped Polycrystalline Graphene: A Molecular Dynamics Study, *Phys. E*, 2018, **99**, 24–36, DOI: 10.1016/j.physe.2017.12.036.

105 S. Fazeli, M. Izadifar, J. S. Dolado, A. Ramazani and S. K. Sadrnezhaad, Atomistic Study of the Effect of Crystallographic Orientation on the Twinning and Detwinning Behavior of NiTi Shape Memory Alloys, *Comput. Mater. Sci.*, 2022, **203**, 111080, DOI: 10.1016/j.commatsci.2021.111080.

106 R. Abadi, A. H. Nezhad Shirazi, M. Izadifar, M. Sepahi and T. Rabczuk, Fabrication of Nanopores in Polycrystalline Boron-Nitride Nanosheet by Using Si, SiC and Diamond Clusters Bombardment, *Comput. Mater. Sci.*, 2018, **145**, 280–290, DOI: 10.1016/j.commatsci.2017.12.022.

107 R. Abadi, M. Izadifar, M. Sepahi, N. Alajlan and T. Rabczuk, Computational Modeling of Graphene Nanopore for Using in DNA Sequencing Devices, *Phys. E*, 2018, **103**, 403–416, DOI: 10.1016/j.physe.2018.05.003.

108 Y. Bahari, B. Mortazavi, A. Rajabpour, X. Zhuang and T. Rabczuk, Application of Two-Dimensional Materials as Anodes for Rechargeable Metal-Ion Batteries: A Comprehensive Perspective from Density Functional Theory Simulations, *Energy Storage Mater.*, 2021, **35**, 203–282, DOI: 10.1016/j.ensm.2020.11.004.

109 A. J. R. Hensley, K. Ghale, C. Rieg, T. Dang, E. Anderst, F. Studt, C. T. Campbell, J.-S. McEwen and Y. Xu, DFT-Based Method for More Accurate Adsorption Energies: An

Adaptive Sum of Energies from RPBE and vdW Density Functionals, *J. Phys. Chem. C*, 2017, **121**(9), 4937–4945, DOI: 10.1021/acs.jpcc.6b10187.

110 M. Izadifar, N. Ukrainczyk and E. Koenders, Atomistic Insights into Silicate Dissolution of Metakaolinite under Alkaline Conditions: Ab Initio Quantum Mechanical Investigation, *Langmuir*, 2024, **40**(37), 19332–19342, DOI: 10.1021/acs.langmuir.4c00890.

111 M. Izadifar, N. C. Valencia, P. Xiao, N. Ukrainczyk and E. Koenders, 3D Off-Lattice Coarse-Grained Monte Carlo Simulations for Nucleation of Alkaline Aluminosilicate Gels, *Materials*, 2023, **16**(5), 1863, DOI: 10.3390/ma16051863.

112 N. C. Valencia, M. Izadifar, N. Ukrainczyk and E. Koenders, Coarse-Grained Monte Carlo Simulations with Octree Cells for Geopolymer Nucleation at Different pH Values, *Materials*, 2024, **17**(1), 95, DOI: 10.3390/ma17010095.

113 M. Izadifar, N. Ukrainczyk and E. Koenders, Coarse-Grained Monte Carlo Simulations of Graphene-Enhanced Geopolymer Nanocomposite Nucleation, *Nanomaterials*, 2025, **15**(4), 289, DOI: 10.3390/nano15040289.

114 M. Izadifar, P. Thissen, A. Steudel, R. Kleeberg, S. Kaufhold, J. Kaltenbach, R. Schuhmann, F. Dehn and K. Emmerich, Comprehensive Examination of Dehydroxylation of Kaolinite, Disordered Kaolinite, and Dickite: Experimental Studies and Density Functional Theory, *Clays Clay Miner.*, 2020, **68**(4), 319–333, DOI: 10.1007/s42860-020-00082-w.

115 B. H. Cho, W. Chung and B. H. Nam, Molecular Dynamics Simulation of Calcium-Silicate-Hydrate for Nano-Engineered Cement Composites—A Review, *Nanomaterials*, 2020, **10**(11), 2158, DOI: 10.3390/nano10112158.

116 D. Bish and R. B. Dreele, Rietveld Refinement of Non-Hydrogen Atomic Positions in Kaolinite, *Clays Clay Miner.*, 1989, **37**, 289–296, DOI: 10.1346/CCMN.1989.0370401.

117 S. Sperinck, P. Raiteri, N. Marks and K. Wright, Dehydroxylation of Kaolinite to Metakaolin—a Molecular Dynamics Study, *J. Mater. Chem.*, 2011, **21**(7), 2118–2125, DOI: 10.1039/C0JM01748E.

118 B. Ilic, A. Mitrović and M. Ljiljana, Thermal Treatment of Kaolin Clay to Obtain Metakaolin, *Hem. Ind.*, 2010, **64**, 351–356, DOI: 10.2298/HEMIND100322014I.

119 L. Piga, Thermogravimetry of a Kaolinite-Alunite Ore, *Thermochim. Acta*, 1995, **265**, 177–187, DOI: 10.1016/0040-6031(95)02429-6.

120 A. Shvarzman, K. Kovler, G. S. Grader and G. E. Shter, The Effect of Dehydroxylation/Amorphization Degree on Pozzolanic Activity of Kaolinite, *Cem. Concr. Res.*, 2003, **33**(3), 405–416, DOI: 10.1016/S0008-8846(02)00975-4.

121 T. Hanein, K.-C. Thienel, F. Zunino, A. T. M. Marsh, M. Maier, B. Wang, M. Canut, M. C. G. Juenger, M. Ben Haha, F. Avet, A. Parashar, L. A. Al-Jaberi, R. S. Almenares-Reyes, A. Alujas-Diaz, K. L. Scrivener, S. A. Bernal, J. L. Provis, T. Sui, S. Bishnoi and F. Martirena-Hernández, Clay Calcination Technology: State-of-the-Art Review by the RILEM TC 282-CCL, *Mater. Struct.*, 2021, **55**(1), 3, DOI: 10.1617/s11527-021-01807-6.

122 N. Garg and J. Skibsted, Dissolution Kinetics of Calcined Kaolinite and Montmorillonite in Alkaline Conditions: Evidence for Reactive Al(V) Sites, *J. Am. Ceram. Soc.*, 2019, **102**(12), 7720–7734, DOI: 10.1111/jace.16663.

123 T. Hanzlicek and M. Steinerova-Vondrakova, Investigation of Dissolution of Aluminosilicates in Aqueous Alkaline Solution under Laboratory Conditions, *Ceramics*, 2002, **46**(3), 97–103.

124 M. Bellotto, A. Gualtieri, G. Artioli and S. M. Clark, Kinetic Study of the Kaolinite-Mullite Reaction Sequence. Part I: Kaolinite Dehydroxylation, *Phys. Chem. Miner.*, 1995, **22**(4), 207–217, DOI: 10.1007/BF00202253.

125 D. de Ligny and A. Navrotsky, Energetics of Kaolin Polymorphs, *Am. Mineral.*, 1999, **84**(4), 506–516, DOI: 10.2138/am-1999-0404.

126 P. Ptáček, F. Frajkorová, F. Šoukal and T. Opravil, Kinetics and Mechanism of Three Stages of Thermal Transformation of Kaolinite to Metakaolinite, *Powder Technol.*, 2014, **264**, 439–445, DOI: 10.1016/j.powtec.2014.05.047.

127 J. Davidovits, Geopolymers: Ceramic-like Inorganic Polymers, *J. Ceram. Sci. Tech.*, 2017, **8**, 335–350, DOI: 10.4416/JCST2017-00038.

128 N. J. Coleman and W. R. Mcwhinnie, The Solid State Chemistry of Metakaolin-Blended Ordinary Portland Cement, *J. Mater. Sci.*, 2000, **35**(11), 2701–2710, DOI: 10.1023/A:1004753926277.

129 W. F. Bleam, S. F. Dec and J. S. Frye, 27Al Solid-State Nuclear Magnetic Resonance Study of Five-Coordinate Aluminum in Augelite and Senegalite, *Phys. Chem. Miner.*, 1989, **16**(8), 817–820, DOI: 10.1007/BF00209706.

130 M. L. Granizo, S. Alonso, M. T. Blanco-Varela and A. Palomo, Alkaline Activation of Metakaolin: Effect of Calcium Hydroxide in the Products of Reaction, *J. Am. Ceram. Soc.*, 2002, **85**(1), 225–231, DOI: 10.1111/j.1151-2916.2002.tb00070.x.

131 C. Panagiotopoulou, E. Kontori, T. Perraki and G. Kakali, Dissolution of Aluminosilicate Minerals and By-Products in Alkaline Media, *J. Mater. Sci.*, 2007, **42**(9), 2967–2973, DOI: 10.1007/s10853-006-0531-8.

132 L. Weng and K. Sagoe-Crentsil, Dissolution Processes, Hydrolysis and Condensation Reactions during Geopolymer Synthesis: Part I—Low Si/Al Ratio Systems, *J. Mater. Sci.*, 2007, **42**(9), 2997–3006, DOI: 10.1007/s10853-006-0820-2.

133 A. Hajimohammadi and J. S. J. van Deventer, Dissolution Behaviour of Source Materials for Synthesis of Geopolymer Binders: A Kinetic Approach, *Int. J. Miner. Process.*, 2016, **153**, 80–86, DOI: 10.1016/j.minpro.2016.05.014.

134 S. Alonso and A. Palomo, Alkaline Activation of Metakaolin and Calcium Hydroxide Mixtures: Influence of Temperature, Activator Concentration and Solids Ratio, *Mater. Lett.*, 2001, **47**(1), 55–62, DOI: 10.1016/S0167-577X(00)00212-3.

135 S. Boonjaeng, P. Chindaprasirt and K. Pimraksa, Lime-Calcined Clay Materials with Alkaline Activation: Phase Development and Reaction Transition Zone, *Appl. Clay Sci.*, 2014, **95**, 357–364, DOI: 10.1016/j.clay.2014.05.002.

136 P. Romero and N. Garg, Evolution of Kaolinite Morphology upon Exfoliation and Dissolution: Evidence for Nanoscale Layer Thinning in Metakaolin, *Appl. Clay Sci.*, 2022, **222**, 106486, DOI: 10.1016/j.clay.2022.106486.

137 K. L. Konan, C. Peyratout, A. Smith, J.-P. Bonnet, S. Rossignol and S. Oyetola, Comparison of Surface Properties between Kaolin and Metakaolin in Concentrated Lime Solutions, *J. Colloid Interface Sci.*, 2009, **339**(1), 103–109, DOI: 10.1016/j.jcis.2009.07.019.

138 S. Scherb, M. Maier, N. Beuntner, K.-C. Thienel and J. Neubauer, Reaction Kinetics during Early Hydration of Calcined Phyllosilicates in Clinker-Free Model Systems, *Cem. Concr. Res.*, 2021, **143**, 106382, DOI: 10.1016/j.cemconres.2021.106382.

139 H. Wang, H. Wu, Z. Xing, R. Wang and S. Dai, The Effect of Various Si/Al, Na/Al Molar Ratios and Free Water on Micromorphology and Macro-Strength of Metakaolin-Based Geopolymer, *Materials*, 2021, **14**(14), 3845, DOI: 10.3390/ma14143845.

140 X. Chen, B. Jin and P. Suraneni, Understanding the Dissolution of Metakaolin in Sodium Hydroxide Solutions, *Mater. Struct.*, 2024, **57**(4), 102, DOI: 10.1617/s11527-024-02365-3.

141 L. Weng, K. Sagoe-Crentsil, T. Brown and S. Song, Effects of Aluminates on the Formation of Geopolymers, *Mater. Sci. Eng., B*, 2005, **117**(2), 163–168, DOI: 10.1016/j.mseb.2004.11.008.

142 N. Granizo, A. Palomo and A. Fernandez-Jiménez, Effect of Temperature and Alkaline Concentration on Metakaolin Leaching Kinetics, *Ceram. Int.*, 2014, **40**(7, Part A), 8975–8985, DOI: 10.1016/j.ceramint.2014.02.071.

143 T. Rocha, S. da, D. P. Dias, F. C. C. França, R. R. Guerra, S. de, L. R. Marques, C. da and O. de, Metakaolin-Based Geopolymer Mortars with Different Alkaline Activators (Na^+ and K^+), *Constr. Build. Mater.*, 2018, **178**, 453–461, DOI: 10.1016/j.conbuildmat.2018.05.172.

144 S. Scherb, M. Köberl, N. Beuntner, K.-C. Thienel and J. Neubauer, Reactivity of Metakaolin in Alkaline Environment: Correlation of Results from Dissolution Experiments with XRD Quantifications, *Materials*, 2020, **13**(10), 2214, DOI: 10.3390/ma13102214.

145 A. Ali Siyal, R. M. S. R. Mohamed, R. Shamsuddin and M. Baharudin Ridzuan, A Comprehensive Review of Synthesis Kinetics and Formation Mechanism of Geopolymers, *RSC Adv.*, 2024, **14**(1), 446–462, DOI: 10.1039/D3RA06205H.

146 A. Fernández-Jiménez and A. Palomo, Characterisation of Fly Ashes. Potential Reactivity as Alkaline Cements, *Fuel*, 2003, **82**(18), 2259–2265, DOI: 10.1016/S0016-2361(03)00194-7.

147 J. L. Provis and J. S. J. van Deventer, Geopolymerisation Kinetics. 2. Reaction Kinetic Modelling, *Chem. Eng. Sci.*, 2007, **62**(9), 2318–2329, DOI: 10.1016/j.ces.2007.01.028.

148 J. L. Provis, P. A. Walls and J. S. J. van Deventer, Geopolymerisation Kinetics. 3. Effects of Cs and Sr Salts, *Chem. Eng. Sci.*, 2008, **63**(18), 4480–4489, DOI: 10.1016/j.ces.2008.06.008.

149 P. Duxson, J. L. Provis, G. C. Lukey, S. W. Mallicoat, W. M. Kriven and J. S. J. van Deventer, Understanding the Relationship between Geopolymer Composition, Microstructure and Mechanical Properties, *Colloids Surf., A*, 2005, **269**(1), 47–58, DOI: 10.1016/j.colsurfa.2005.06.060.

150 N. Werling, F. Dehn, F. Krause, A. Steudel, R. Schuhmann and K. Emmerich, Solubility of Precursors and Carbonation of Waterglass-Free Geopolymers, *Clays Clay Miner.*, 2020, **68**(5), 524–531, DOI: 10.1007/s42860-020-00096-4.

151 A. Palomo, P. Krivenko, I. Garcia-Lodeiro, E. Kavalerova, O. Maltseva and A. Fernández-Jiménez, A Review on Alkaline Activation: New Analytical Perspectives, *Mater. Constr.*, 2014, **64**(315), e022–e022, DOI: 10.3989/mc.2014.00314.

152 X. Wang, W. Yang, H. Liu, P. Zhu, N. Zong and J. Feng, Strength and Microstructural Analysis of Geopolymer Prepared with Recycled Geopolymer Powder, *J. Wuhan Univ. Technol., Mater. Sci. Ed.*, 2021, **36**(3), 439–445, DOI: 10.1007/s11595-021-2428-4.

153 A. Gharzouni, E. Joussein, B. Samet, S. Baklouti and S. Rossignol, Effect of the Reactivity of Alkaline Solution and Metakaolin on Geopolymer Formation, *J. Non-Cryst. Solids*, 2015, **410**, 127–134, DOI: 10.1016/j.jnoncrysol.2014.12.021.

154 A. Gharzouni, E. Joussein, B. Samet, S. Baklouti, S. Pronier, I. Sobrados, J. Sanz and S. Rossignol, The Effect of an Activation Solution with Siliceous Species on the Chemical Reactivity and Mechanical Properties of Geopolymers, *J. Sol-Gel Sci. Technol.*, 2015, **73**(1), 250–259, DOI: 10.1007/s10971-014-3524-0.

155 C. Tippayasam, P. Balyore, P. Thavorniti, E. Kamseu, C. Leonelli, P. Chindaprasirt and D. Chaysuwan, Potassium Alkali Concentration and Heat Treatment Affected Metakaolin-Based Geopolymer, *Constr. Build. Mater.*, 2016, **104**, 293–297, DOI: 10.1016/j.conbuildmat.2015.11.027.

156 N. Beuntner and C. Thienel, *Solubility and Kinetics of Calcined Clay: Study of Interaction by Pore Solution*; 2016.

157 K. M. L. Alventosa and C. E. White, The Effects of Calcium Hydroxide and Activator Chemistry on Alkali-Activated Metakaolin Pastes, *Cem. Concr. Res.*, 2021, **145**, 106453, DOI: 10.1016/j.cemconres.2021.106453.

158 K. Weise, L. M. Endell, N. Ukrainczyk and E. Koenders, Pozzolanic Metakaolin Reactivity: Time-Dependent Influence of Calcium Hydroxide, Alkali Hydroxides, and Sulfates, *Constr. Build. Mater.*, 2024, **431**, 136534, DOI: 10.1016/j.conbuildmat.2024.136534.

159 F. Bellmann and J. Stark, Activation of Blast Furnace Slag by a New Method, *Cem. Concr. Res.*, 2009, **39**(8), 644–650, DOI: 10.1016/j.cemconres.2009.05.012.

160 C. Shi, D. Roy and P. Krivenko, *Alkali-Activated Cements and Concretes*, CRC Press, London, 2014, DOI: 10.1201/9781482266900.

161 C. Shi and J. Qian, High Performance Cementing Materials from Industrial Slags—a Review, *Resour., Conserv. Recycl.*, 2000, **29**(3), 195–207, DOI: 10.1016/S0921-3449(99)00060-9.

162 A. A. Gonçalves Junior, E. I. Jussiani, A. C. Andrello, R. D. Vanderlei and B. M. Toralles, Ecoefficient Cementitious

Materials with High Levels of Portland Cement Replacement Using Blast Furnace Slag, *J. Mater. Civ. Eng.*, 2024, **36**(8), 04024229, DOI: 10.1061/JMCEE7.MTENG-17320.

163 G. J. Osborne, Durability of Portland Blast-Furnace Slag Cement Concrete, *Cem. Concr. Compos.*, 1999, **21**(1), 11–21, DOI: 10.1016/S0958-9465(98)00032-8.

164 K. Shimoda and K. Saito, Detailed Structure Elucidation of the Blast Furnace Slag by Molecular Dynamics Simulation, *ISIJ Int.*, 2007, **47**(9), 1275–1279, DOI: 10.2355/isijinternational.47.1275.

165 B. Lin, H. Wang, X. Zhu, Q. Liao and B. Ding, Crystallization Properties of Molten Blast Furnace Slag at Different Cooling Rates, *Appl. Therm. Eng.*, 2016, **96**, 432–440, DOI: 10.1016/j.applthermaleng.2015.11.075.

166 W. Liu, H. Wu, X. Xing, J. Wang, Q. Xue and H. Zuo, Confocal Scanning Laser Microscopy Investigation of Crystallization Behavior of Hot Blast Furnace Slag, *J. Non-Cryst. Solids*, 2023, **600**, 122013, DOI: 10.1016/j.jnoncrysol.2022.122013.

167 Q. Yuelin, L. Hao and Y. Yanhua, Structure Evolution of Blast Furnace Slag with High Al2O3 Content and 5 Mass% TiO2 via Molecular Dynamics Simulation and Fourier Transform Infrared Spectroscopy, *Metall. Res. Technol.*, 2018, **115**(1), 113, DOI: 10.1051/metal/2017090.

168 D. Liang, Z. Yan, X. Lv, J. Zhang and C. Bai, Transition of Blast Furnace Slag from Silicate-Based to Aluminate-Based: Structure Evolution by Molecular Dynamics Simulation and Raman Spectroscopy, *Metall. Mater. Trans. B*, 2017, **48**(1), 573–581, DOI: 10.1007/s11663-016-0855-y.

169 S. Rahemipoor, C. Kuenzel, T. Valdemārs Eiduks, A. Shishkin, M. Izadifar, N. Ukrainczyk, E. Koenders and N. Ranjbar, Surface-Engineered Cenospheres Encapsulating Phase Change Materials for Functional Cementitious Composites, *Adv. Sci.*, 2025, 2417350, DOI: 10.1002/advs.202417350.

170 S. Rahemipoor, C. Kuenzel, T. Valdemārs Eiduks, A. Shishkin, M. Izadifar, N. Ukrainczyk, E. Koenders and N. Ranjbar, Surface-Engineered Cenospheres Encapsulating Phase Change Materials for Functional Cementitious Composites (Adv. Sci. 26/2025), *Adv. Sci.*, 2025, **12**(26), 2570199, DOI: 10.1002/advs.202570199.

171 P. Hewlett, *Lea's Chemistry of Cement and Concrete*, 2003.

172 G. L. Golewski, The Role of Pozzolanic Activity of Siliceous Fly Ash in the Formation of the Structure of Sustainable Cementitious Composites, *Sustainable Chem.*, 2022, **3**(4), 520–534, DOI: 10.3390/suschem3040032.

173 M. D. A. Thomas, *Optimizing the Use of Fly Ash in Concrete*, Portland Cement Association, 2007.

174 M. I. A and S. K. N, 3D Printed Concrete Using Portland Pozzolana Cement - Fly Ash Based, *E3S Web Conf.*, 2024, **529**, 01019, DOI: 10.1051/e3sconf/202452901019.

175 B. Yin, T. Kang, J. Kang and Y. Chen, Analysis of Active Ion-Leaching Behavior and the Reaction Mechanism During Alkali Activation of Low-Calcium Fly Ash, *Int. J. Concr. Struct. Mater.*, 2018, **12**(1), 50, DOI: 10.1186/s40069-018-0282-3.

176 L. P. Kudva, G. Nayak, K. K. Shetty and H. K. Sugandhini, Mechanical Properties of Fiber-Reinforced High-Volume Fly-Ash-Based Cement Composite—A Long-Term Study, *Sustainability*, 2023, **15**(17), 13128, DOI: 10.3390/su151713128.

177 W. Zhang, S. Wang, L. Zhao, J. Ran, W. Kang, C. Feng and J. Zhu, Investigation of Low-Calcium Circulating Fluidized Bed Fly Ash on the Mechanical Strength and Microstructure of Cement-Based Material, *Crystals*, 2022, **12**(3), 400, DOI: 10.3390/cryst12030400.

178 R. Snellings, H. Kazemi-Kamyab, P. Nielsen and L. Van den Abeele, Classification and Milling Increase Fly Ash Pozzolanic Reactivity, *Front. Built Environ.*, 2021, 7, DOI: 10.3389/fbuil.2021.670996.

179 A. Kumar, N. Bheel, I. Ahmed, S. H. Rizvi, R. Kumar and A. A. Jhatial, Effect of Silica Fume and Fly Ash as Cementitious Material on Hardened Properties and Embodied Carbon of Roller Compacted Concrete, *Environ. Sci. Pollut. Res.*, 2022, **29**(1), 1210–1222, DOI: 10.1007/s11356-021-15734-0.

180 I. Amer, M. Kohail, M. S. El-Feky, A. Rashad and M. A. Khalaf, A Review on Alkali-Activated Slag Concrete, *Ain Shams Eng. J.*, 2021, **12**(2), 1475–1499, DOI: 10.1016/j.asej.2020.12.003.

181 Q. Fu, M. Bu, Z. Zhang, W. Xu, Q. Yuan and D. Niu, Hydration Characteristics and Microstructure of Alkali-Activated Slag Concrete: A Review, *Engineering*, 2023, **20**, 162–179, DOI: 10.1016/j.eng.2021.07.026.

182 P. Zhang, K. Wang, Q. Li, J. Wang and Y. Ling, Fabrication and Engineering Properties of Concretes Based on Geopolymers/Alkali-Activated Binders - A Review, *J. Cleaner Prod.*, 2020, **258**, 120896, DOI: 10.1016/j.jclepro.2020.120896.

183 W. Lu, J. Li, G. Qi, X. Hu, Q. Zhang, M. Wang and M. Zhang, Preparation and Properties of Zeolite-Fly Ash-Slag Composite Porous Materials: CO2 Adsorption Performance and Mechanical Property, *Environ. Sci. Pollut. Res.*, 2023, **30**(10), 27303–27314, DOI: 10.1007/s11356-022-24027-z.

184 M. C. G. Juenger, F. Winnefeld, J. L. Provis and J. H. Ideker, Advances in Alternative Cementitious Binders, *Cem. Concr. Res.*, 2011, **41**(12), 1232–1243, DOI: 10.1016/j.cemconres.2010.11.012.

185 M. B. Haha, B. Lothenbach, G. Le Saout and F. Winnefeld, Influence of Slag Chemistry on the Hydration of Alkali-Activated Blast-Furnace Slag—Part I: Effect of MgO, *Cem. Concr. Res.*, 2011, **41**(9), 955–963, DOI: 10.1016/j.cemconres.2011.05.002.

186 M. B. Haha, B. Lothenbach, G. Le Saout and F. Winnefeld, Influence of Slag Chemistry on the Hydration of Alkali-Activated Blast-Furnace Slag—Part II: Effect of Al2O3, *Cem. Concr. Res.*, 2012, **42**(1), 74–83, DOI: 10.1016/j.cemconres.2011.08.005.

187 A. R. Brough and A. Atkinson, Sodium Silicate-Based, Alkali-Activated Slag Mortars: Part I. Strength, Hydration and Microstructure, *Cem. Concr. Res.*, 2002, **32**(6), 865–879, DOI: 10.1016/S0008-8846(02)00717-2.

188 F. Collins and J. G. Sanjayan, Effects of Ultra-Fine Materials on Workability and Strength of Concrete Containing Alkali-Activated Slag as the Binder, *Cem. Concr. Res.*, 1999, **29**(3), 459–462, DOI: 10.1016/S0008-8846(98)00237-3.

189 S.-D. Wang, K. L. Scrivener and P. L. Pratt, Factors Affecting the Strength of Alkali-Activated Slag, *Cem. Concr. Res.*, 1994, **24**(6), 1033–1043, DOI: 10.1016/0008-8846(94)90026-4.

190 M. Ben Haha, G. Le Saout, F. Winnefeld and B. Lothenbach, Influence of Activator Type on Hydration Kinetics, Hydrate Assemblage and Microstructural Development of Alkali Activated Blast-Furnace Slags, *Cem. Concr. Res.*, 2011, **41**(3), 301–310, DOI: 10.1016/j.cemconres.2010.11.016.

191 B. Talling, *Effect of Curing Conditions on Alkali-Activated Slags*. 1989.

192 X. Ke, S. A. Bernal and J. L. Provis, Controlling the Reaction Kinetics of Sodium Carbonate-Activated Slag Cements Using Calcined Layered Double Hydroxides, *Cem. Concr. Res.*, 2016, **81**, 24–37, DOI: 10.1016/j.cemconres.2015.11.012.

193 S. Song, D. Sohn, H. M. Jennings and T. O. Mason, Hydration of Alkali-Activated Ground Granulated Blast Furnace Slag, *J. Mater. Sci.*, 2000, **35**(1), 249–257, DOI: 10.1023/A:1004742027117.

194 S. A. Bernal, R. San Nicolas, R. J. Myers, R. Mejía de Gutiérrez, F. Puertas, J. S. J. van Deventer and J. L. Provis, MgO Content of Slag Controls Phase Evolution and Structural Changes Induced by Accelerated Carbonation in Alkali-Activated Binders, *Cem. Concr. Res.*, 2014, **57**, 33–43, DOI: 10.1016/j.cemconres.2013.12.003.

195 J. Bijen and E. Niël, Supersulphated Cement from Blastfurnace Slag and Chemical Gypsum Available in the Netherlands and Neighbouring Countries, *Cem. Concr. Res.*, 1981, **11**(3), 307–322, DOI: 10.1016/0008-8846(81)90104-6.

196 H. G. Midgley and K. Pettifer, The Micro Structure of Hydrated Super Sulphated Cement, *Cem. Concr. Res.*, 1971, **1**(1), 101–104, DOI: 10.1016/0008-8846(71)90086-X.

197 D. K. Dutta and P. C. Borthakur, Activation of Low Lime High Alumina Granulated Blast Furnace Slag by Anhydrite, *Cem. Concr. Res.*, 1990, **20**(5), 711–722, DOI: 10.1016/0008-8846(90)90005-I.

198 V. P. Mehrotra, A. S. R. Sai and P. C. Kapur, Plaster of Paris Activated Supersulfated Slag Cement, *Cem. Concr. Res.*, 1982, **12**(4), 463–473, DOI: 10.1016/0008-8846(82)90061-8.

199 L. Dongxu, W. Xuequan, S. Jinlin and W. Yujiang, The Influence of Compound Admixtures on the Properties of High-Content Slag Cement, *Cem. Concr. Res.*, 2000, **30**(1), 45–50, DOI: 10.1016/S0008-8846(99)00210-0.

200 X. Fu, W. Hou, C. Yang, D. Li and X. Wu, Studies on Portland Cement with Large Amount of Slag, *Cem. Concr. Res.*, 2000, **30**(4), 645–649, DOI: 10.1016/S0008-8846(00)00208-8.

201 A. Gruskovnjak, B. Lothenbach, F. Winnefeld, R. Figi, S.-C. Ko, M. Adler and U. Mäder, Hydration Mechanisms of Super Sulphated Slag Cement, *Cem. Concr. Res.*, 2008, **38**(7), 983–992, DOI: 10.1016/j.cemconres.2008.03.004.

202 S. Kucharczyk, J. Deja and Z. Maciej, Effect of Slag Reactivity Influenced by Alumina Content on Hydration of Composite Cements, *J. Adv. Concr. Technol.*, 2016, **14**, 535–547, DOI: 10.3151/jact.14.535.

203 N. H. Jamil, M. M. A. B. Abdullah, W. M. A. W. Ibrahim, R. Rahim, A. V. Sandu, P. Vizureanu, J. Castro-Gomes and J. M. Gómez-Soberón, Effect of Sintering Parameters on Microstructural Evolution of Low Sintered Geopolymer Based on Kaolin and Ground-Granulated Blast-Furnace Slag, *Crystals*, 2022, **12**(11), 1553, DOI: 10.3390/cryst12111553.

204 Q. Liu, Z. Chen, Z. M. El-Bahy, P. Wang, S. N. Abdou, M. M. Ibrahim, Y. Wan, J. Wang, H. Li, L. Li and H. Wang, Alkali-Hydrothermal Activation of Tailings with Red Mud as a Supplementary Alkali Source to Synthesize One-Part Geopolymer, *Adv. Compos. Hybrid Mater.*, 2023, **6**(4), 132, DOI: 10.1007/s42114-023-00707-3.

205 Y. Wang, L. E. Burris, C. R. Shearer, R. D. Hooton and P. Suraneni, Characterization and Reactivity of Size-Fractionated Unconventional Fly Ashes, *Mater. Struct.*, 2023, **56**(3), 49, DOI: 10.1617/s11527-023-02140-w.

206 P. K. Sharma, J. P. Singh and A. Kumar, Effect of Particle Size on Physical and Mechanical Properties of Fly Ash Based Geopolymers, *Trans. Indian Inst. Met.*, 2019, **72**(5), 1323–1337, DOI: 10.1007/s12666-019-01628-w.

207 H. Wang, Y. Wang, X. Liu and Z. Zhang, Leaching Kinetics and Reactivity Evaluation of Fly Ash Based on the Synergistic Effect of Alkali and Sulfate, *J. Build. Eng.*, 2023, **80**, 108041, DOI: 10.1016/j.jobe.2023.108041.

208 C. Kuenzel and N. Ranjbar, Dissolution Mechanism of Fly Ash to Quantify the Reactive Aluminosilicates in Geopolymerisation, *Resour., Conserv. Recycl.*, 2019, **150**, 104421, DOI: 10.1016/j.resconrec.2019.104421.

209 K. L. Aughenbaugh, P. Stutzman and M. C. G. Juenger, Identifying Glass Compositions in Fly Ash, *Front. Mater.*, 2016, 3, DOI: 10.3389/fmats.2016.00001.

210 M. Nodehi and V. M. Taghvaee, Alkali-Activated Materials and Geopolymer: A Review of Common Precursors and Activators Addressing Circular Economy, *Circ. Econ. Sustainability*, 2022, **2**(1), 165–196, DOI: 10.1007/s43615-021-00029-w.

211 Q. Zeng and K. Li, Reaction and Microstructure of Cement–Fly-Ash System, *Mater. Struct.*, 2015, **48**(6), 1703–1716, DOI: 10.1617/s11527-014-0266-y.

212 T. Oey, A. Kumar, I. Pignatelli, Y. Yu, N. Neithalath, J. W. Bullard, M. Bauchy and G. Sant, Topological Controls on the Dissolution Kinetics of Glassy Aluminosilicates, *J. Am. Ceram. Soc.*, 2017, **100**(12), 5521–5527, DOI: 10.1111/jace.15122.

213 M. Moesgaard, D. Herfort, J. Skibsted and Y. Yue, Calcium Aluminosilicate Glasses as Supplementary Cementitious Materials, *Glass Technol.:Eur. J. Glass Sci. Technol., Part A*, 2010, **51**(5), 183–190.

214 P. T. Durdziński, R. Snellings, C. F. Dunant, M. B. Haha and K. L. Scrivener, Fly Ash as an Assemblage of Model Ca–Mg–Na-Aluminosilicate Glasses, *Cem. Concr. Res.*, 2015, **78**, 263–272, DOI: 10.1016/j.cemconres.2015.08.005.

215 P. T. Durdziński, C. F. Dunant, M. B. Haha and K. L. Scrivener, A New Quantification Method Based on

SEM-EDS to Assess Fly Ash Composition and Study the Reaction of Its Individual Components in Hydrating Cement Paste, *Cem. Concr. Res.*, 2015, **73**, 111–122, DOI: 10.1016/j.cemconres.2015.02.008.

216 S. Kucharczyk, M. Zajac, C. Stabler, R. M. Thomsen, M. Ben Haha, J. Skibsted and J. Deja, Structure and Reactivity of Synthetic CaO-Al2O3-SiO2 Glasses, *Cem. Concr. Res.*, 2019, **120**, 77–91, DOI: 10.1016/j.cemconres.2019.03.004.

217 K. L. Aughenbaugh, R. T. Chancey, P. Stutzman, M. C. Juenger and D. W. Fowler, An Examination of the Reactivity of Fly Ash in Cementitious Pore Solutions, *Mater. Struct.*, 2013, **46**(5), 869–880, DOI: 10.1617/s11527-012-9939-6.

218 A. Fernández-Jiménez and F. Puertas, Effect of Activator Mix on the Hydration and Strength Behaviour of Alkali-Activated Slag Cements, *Adv. Cem. Res.*, 2003, **15**(3), 129–136, DOI: 10.1680/adcr.2003.15.3.129.

219 A. Fernández-Jiménez and F. Puertas, Setting of Alkali-Activated Slag Cement. Influence of Activator Nature, *Adv. Cem. Res.*, 2001, **13**(3), 115–121, DOI: 10.1680/adcr.2001.13.3.115.

220 A. Fernández-Jiménez and A. Palomo, Composition and Microstructure of Alkali Activated Fly Ash Binder: Effect of the Activator, *Cem. Concr. Res.*, 2005, **35**(10), 1984–1992, DOI: 10.1016/j.cemconres.2005.03.003.

221 X. Guo, H. Shi and W. A. Dick, Compressive Strength and Microstructural Characteristics of Class C Fly Ash Geopolymer, *Cem. Concr. Compos.*, 2010, **32**(2), 142–147, DOI: 10.1016/j.cemconcomp.2009.11.003.

222 D. Ravikumar, S. Peethamparan and N. Neithalath, Structure and Strength of NaOH Activated Concretes Containing Fly Ash or GGBFS as the Sole Binder, *Cem. Concr. Compos.*, 2010, **32**(6), 399–410, DOI: 10.1016/j.cemconcomp.2010.03.007.

223 M. Criado, A. Fernández-Jiménez and A. Palomo, Alkali Activation of Fly Ash: Effect of the SiO2/Na2O Ratio, *Microporous Mesoporous Mater.*, 2007, **106**(1), 180–191, DOI: 10.1016/j.micromeso.2007.02.055.

224 A. Hajimohammadi, J. L. Provis and J. S. J. van Deventer, The Effect of Silica Availability on the Mechanism of Geopolymerisation, *Cem. Concr. Res.*, 2011, **41**(3), 210–216, DOI: 10.1016/j.cemconres.2011.02.001.

225 A. R. Brough, M. Holloway, J. Sykes and A. Atkinson, Sodium Silicate-Based Alkali-Activated Slag Mortars: Part II. The Retarding Effect of Additions of Sodium Chloride or Malic Acid, *Cem. Concr. Res.*, 2000, **30**(9), 1375–1379, DOI: 10.1016/S0008-8846(00)00356-2.

226 J. L. Provis and S. A. Bernal, Geopolymers and Related Alkali-Activated Materials, *Annu. Rev. Mater. Res.*, 2014, **44**(44), 299–327, DOI: 10.1146/annurev-matsci-070813-113515.

227 Y. Briki, M. Zajac, M. B. Haha and K. Scrivener, Factors Affecting the Reactivity of Slag at Early and Late Ages, *Cem. Concr. Res.*, 2021, **150**, 106604, DOI: 10.1016/j.cemconres.2021.106604.

228 F. Yan, K. Luo, J. Ye, W. Zhang, J. Chen, X. Ren, Z. Liu and J. Li, Leaching Kinetics and Dissolution Model of Steel Slag in NaOH Solution, *Constr. Build. Mater.*, 2024, **434**, 136743, DOI: 10.1016/j.conbuildmat.2024.136743.

229 D. Ravikumar and N. Neithalath, Reaction Kinetics in Sodium Silicate Powder and Liquid Activated Slag Binders Evaluated Using Isothermal Calorimetry, *Thermochim. Acta*, 2012, **546**, 32–43, DOI: 10.1016/j.tca.2012.07.010.

230 S. A. Bernal, J. L. Provis, R. J. Myers, R. San Nicolas and J. S. J. van Deventer, Role of Carbonates in the Chemical Evolution of Sodium Carbonate-Activated Slag Binders, *Mater. Struct.*, 2015, **48**(3), 517–529, DOI: 10.1617/s11527-014-0412-6.

231 C. Shi and R. L. Day, Some Factors Affecting Early Hydration of Alkali-Slag Cements, *Cem. Concr. Res.*, 1996, **26**(3), 439–447, DOI: 10.1016/S0008-8846(96)85031-9.

232 B. S. Gebregziabiher, R. J. Thomas and S. Peethamparan, Temperature and Activator Effect on Early-Age Reaction Kinetics of Alkali-Activated Slag Binders, *Constr. Build. Mater.*, 2016, **113**, 783–793, DOI: 10.1016/j.conbuildmat.2016.03.098.

233 A. Fernandez-Jimenez, F. Puertas and A. Arteaga, Determination of Kinetic Equations of Alkaline Activation of Blast Furnace Slag by Means of Calorimetric Data, *J. Therm. Anal. Calorim.*, 1998, **52**(3), 945–955, DOI: 10.1023/A:1010172204297.

234 T. Y. Qi, G. R. Feng, Y. J. Zhang, J. Guo and Y. X. Guo, The Study on the Activity of Fly Ash in Ca(OH)2 Solution, *Mater. Res. Innovations*, 2015, **19**(sup1), 454–458, DOI: 10.1179/1432891715Z.0000000001591.

235 C. Chen, W. Gong, W. Lutze, I. L. Pegg and J. Zhai, Kinetics of Fly Ash Leaching in Strongly Alkaline Solutions, *J. Mater. Sci.*, 2011, **46**(3), 590–597, DOI: 10.1007/s10853-010-4997-z.

236 I. Wilińska and B. Pacewska, Comparative Investigation of Reactivity of Different Kinds of Fly Ash in Alkaline Media, *J. Therm. Anal. Calorim.*, 2019, **138**(6), 3857–3872, DOI: 10.1007/s10973-019-08296-4.

237 D. Glosser; A. Choudhary; O. B. Isgor and W. J. Weiss Investigation of Reactivity of Fly Ash and Its Effect on Mixture Properties.

238 M. Palacios, M. M. Alonso, C. Varga and F. Puertas, Influence of the Alkaline Solution and Temperature on the Rheology and Reactivity of Alkali-Activated Fly Ash Pastes, *Cem. Concr. Compos.*, 2019, **95**, 277–284, DOI: 10.1016/j.cemconcomp.2018.08.010.

239 E. Deir, B. S. Gebregziabiher and S. Peethamparan, Influence of Starting Material on the Early Age Hydration Kinetics, Microstructure and Composition of Binding Gel in Alkali Activated Binder Systems, *Cem. Concr. Compos.*, 2014, **48**, 108–117, DOI: 10.1016/j.cemconcomp.2013.11.010.

240 G. Deng, Y. He, L. Lu, F. Wang and S. Hu, Comparison between Fly Ash and Slag Slurry in Various Alkaline Environments: Dissolution, Migration, and Coordination State of Aluminum, *ACS Sustainable Chem. Eng.*, 2021, **9**(36), 12109–12119, DOI: 10.1021/acssuschemeng.1c03434.

241 C. E. White, J. L. Provis, T. Proffen, D. P. Riley and J. S. Van Deventer, Combining Density Functional Theory (DFT) and Pair Distribution Function (PDF) Analysis to Solve the Structure of Metastable Materials: The Case of Meta-kaolin, *Phys. Chem. Chem. Phys.*, 2010, **12**(13), 3239–3245, DOI: 10.1039/B922993K.

242 C. E. White, J. L. Provis, T. Proffen and J. S. J. van Deventer, Molecular Mechanisms Responsible for the Structural Changes Occurring during Geopolymerization: Multiscale Simulation, *AIChE J.*, 2012, **58**(7), 2241–2253, DOI: 10.1002/aic.12743.

243 M. Izadifar, N. Ukrainczyk, K. Schönfeld and E. Koenders, Activation Energy of Aluminate Dissolution in Metakaolin: MLFF-Accelerated DFT Study of vdW and Hydration Shell Effects, *Nanoscale Adv.*, 2025, **7**, 4325–4335, DOI: 10.1039/D5NA00103J.

244 B. Mortazavi, Recent Advances in Machine Learning-Assisted Multiscale Design of Energy Materials, *Adv. Energy Mater.*, 2025, **15**(9), 2403876, DOI: 10.1002/aenm.202403876.

245 A. Rajabpour, B. Mortazavi, P. Mirchi, J. El Hajj, Y. Guo, X. Zhuang and S. Merabia, Accurate Estimation of Interfacial Thermal Conductance between Silicon and Diamond Enabled by a Machine Learning Interatomic Potential, *Int. J. Therm. Sci.*, 2025, **214**, 109876, DOI: 10.1016/j.ijthermalsci.2025.109876.

246 A. Kabylda, B. Mortazavi, X. Zhuang and A. Tkatchenko, Mechanical Properties of Nanoporous Graphenes: Transferability of Graph Machine-Learned Force Fields Compared to Local and Reactive Potentials, *Adv. Funct. Mater.*, 2025, **35**(13), 2417891, DOI: 10.1002/adfm.202417891.

247 B. Mortazavi, T. Rabczuk and X. Zhuang, Exploring the Structural Stability, Thermal and Mechanical Properties of Nanoporous Carbon Nitride Nanosheets Using a Transferrable Machine Learning Interatomic Potential, *Comput. Sci. Eng.*, 2025, **1**(1), 5, DOI: 10.1007/s44379-024-00008-6.

248 C. E. White, J. L. Provis, G. J. Kearley, D. P. Riley and J. S. J. van Deventer, Density Functional Modelling of Silicate and Aluminosilicate Dimerisation Solution Chemistry, *Dalton Trans.*, 2011, **40**(6), 1348–1355, DOI: 10.1039/C0DT01042A.

249 W. Sekkal and A. Zaoui, High Strength Metakaolin-Based Geopolymer Reinforced by Pristine and Covalent Functionalized Carbon Nanotubes, *Constr. Build. Mater.*, 2022, **327**, 126910, DOI: 10.1016/j.conbuildmat.2022.126910.

250 Y. Chen, J. S. Dolado, Z. Li, S. Yin, Q. Yu, A. Kostiuchenko and G. Ye, A Molecular Dynamics Study of N–A–S–H Gel with Various Si/Al Ratios, *J. Am. Ceram. Soc.*, 2022, **105**(10), 6462–6474, DOI: 10.1111/jace.18597.

251 F. Hong, C. Liu, M. Wang, X. Ji, M. Wang, Z. Li, D. Hou and M. Li, Molecular Dynamics Study of Surface Alkalization Reaction in High Calcium Systems, *J. Build. Eng.*, 2024, **91**, 109475, DOI: 10.1016/j.jobe.2024.109475.

252 F. Guo, J. Chen, Q. Tang, M. Sun, H. Feng, H. Gao, M. Li and S. Lu, Molecular Dynamics Simulation of the Initial Stage Induction of Alkali-Activated Aluminosilicate Minerals, *RSC Adv.*, 2024, **14**(20), 13972–13983, DOI: 10.1039/D4RA00822G.

253 K. Gong and C. E. White, Time-Dependent Phase Quantification and Local Structure Analysis of Hydroxide-Activated Slag via X-Ray Total Scattering and Molecular Modeling, *Cem. Concr. Res.*, 2022, **151**, 106642, DOI: 10.1016/j.cemconres.2021.106642.

254 K. Gong and C. E. White, Predicting CaO-(MgO)-Al2O3-SiO2 Glass Reactivity in Alkaline Environments from Force Field Molecular Dynamics Simulations, *Cem. Concr. Res.*, 2021, **150**, 106588, DOI: 10.1016/j.cemconres.2021.106588.

255 J. Huang and B. Wang, Structural Evolution and Reaction Mechanisms of Alkali-Activated Slag with Diverse Mg/Si Ratios: A View from the Nanoscale, *Constr. Build. Mater.*, 2024, **457**, 139475, DOI: 10.1016/j.conbuildmat.2024.139475.